



CHAPTER V

CONCLUSIONS

Based on the experimental results, walls with diagonal web reinforcement are believed to perform better than those with similar amounts of conventional web reinforcement. The following conclusions can be drawn from this investigation:

1. The shapes of hysteresis loops of walls with diagonal web reinforcement exhibit less pinching than the wall with conventional reinforcement. Therefore, the energy dissipation capacity of walls with diagonal web reinforcement is superior to that with conventional web reinforcement by about 23% at drift ratio of 1.5%.
2. For the walls tested, the diagonal web reinforcement effectively reduces the shear deformation by approximately 20%. Consequently, the brittle web crushing failure could be deferred, leading to an enhanced performance of the diagonally reinforced walls in comparison with the conventional one.
3. Although the brittle web crushing failure mode is alleviated by the use of diagonal reinforcement, the diagonal bars are subjected to high compressive stresses and tend to buckle. Spalling of the concrete cover in the web accompanies buckling of the web reinforcement and leads to loss of lateral load capacity.
4. The energy dissipation capacity and damping of the specimen with mixed web reinforcement type practically do not differ. Thus, the mixed mode of web reinforcement is quite promising in practice. However, the splice details at the interface between the diagonal and conventional reinforcement are subject to further investigation for efficiency and practicality in construction.
5. The equations for nominal shear strength given in the ACI318-05 Building Code provide over-conservative estimates of the shear strength of walls especially those with diagonal web reinforcement.

In order to clearly understand the influence of diagonal web reinforcement, finite element analyses were performed. The main conclusions are:

1. The effect of buckling of longitudinal bars on the behavior of confined concrete and the difference in stress-strain characteristics of the cover and core concrete in the boundary columns significantly influence the load-displacement envelope. The

ultimate drifts predicted agree reasonably well with the test results, within 10% in general, except for WD150.

2. Finite element analyses confirm the effectiveness of diagonal web reinforcement in reducing the compressive strain in the critical concrete strut in comparison with the conventional one. The reduction is about 23% at the ultimate drift ratio of the latter, thereby deferring web crushing with enhanced performance. The drift capacity also increases in the order of 20%.
3. The finite element analyses indicate that the ultimate drift capacity decreases with an increase in the axial load. However, the results from experiments did not exhibit this behavior and further research is needed to study the wall performance under different levels of axial load.

Finally, a simplified design procedure for walls considering web crushing is proposed. It employs a sectional analysis procedure accounting for shear effect. The peak lateral load capacities predicted agree with the test results within 10%. Furthermore, with this method, not only flexural failure but also web crushing failure can be determined.

TABLES

Table 2.1 Reinforcement details and material properties

Specimen	f'_c (MPa)	Longitudinal reinforcement	f_y/f_u (MPa)	Web reinforcement*	f_y/f_u (MPa)
WC150	27.3	2.57% (8DB16)	574.9/ 646.8	$\rho_n = \rho_v = 0.0080$ (DB10 at 150 mm)	451.3/ 715.5
WD150	40.3	2.57%	574.9/ 646.8	$\rho_d^{**} = 0.0080$ (DB10 at 150 mm)	451.3/ 715.5
WD200	33.7	2.57%	574.9/ 646.8	$\rho_d^{**} = 0.0060$ (DB10 at 200 mm)	451.3/ 715.5
WD170	32.9	2.57%	595.7/ 664.0	$\rho_d^{**} = 0.0070$ (DB10 at 170 mm)	505.9/ 682.7
WCD170	33.9	2.57%	595.7/ 664.0	$\rho_n = \rho_v = \rho_d^{**} = 0.0070$ (DB10 at 170 mm)	505.9/ 682.7
WD170A	32.4	2.57%	595.7/ 664.0	$\rho_n = \rho_v = \rho_d^{**} = 0.0070$ (DB10 at 170 mm)	505.9/ 682.7

* Reinforcement is in 2 curtains, ** Diagonal reinforcement

Table 2.2 Summary of test results

Specimen	Average cracking load (kN)	First yield load (kN)	First yield displacement (mm)	Peak load (kN)	Max. Displ. Ductility	Ultimate Drift	Mode of failure*
WC150	179	675	9.9	870	3.1	2.2%	WC
WD150	293	694	6.7	890	3.9	1.5%	BL
WD200	270	680	8.9	880	3.1	1.6%	BW
WD170	278	680	8.9	980	3.1	2.0%	BL
WCD170	247	697	10.7	890	3.1	2.4%	BL/FL
WD170A	349	800	9.0	1040	3.1	2.0%	BL/FL

*WC: Web crushing, BL: Buckling of longitudinal bars, BW: Buckling of web bars, FL: Fracture of longitudinal bars

Table 2.3 Shear deformation

Specimen	Peak load (kN)	Experimental results		Adjustment for difference in concrete strength		γ_m	ε_y	β	ε_d
		Shear deformation (%)*	Reduction (%)**	Shear deformation (%)*	Reduction (%)**				
WC150	870	27.7	-	27.7	-	0.0086	0.0021	51.9	-0.0034
WD150	890	18.7	32	22.7	18	0.00705	0.0022	53.7	-0.0026
WD170	980	19.8	28	21.7	22	0.00671	0.0023	54.5	-0.0024
WCD170	890	21.8	21	24.3	12	0.00757	0.0023	53.5	-0.0028
WD170A	1040	15.1	45	16.5	40	0.00520	-0.0010	39.5	-0.0031

* percent of total displacement

** compared with specimen WC150

Table 2.4 Lateral load capacity

Specimen	Peak load (kN)	M_n (kN-m)	$V_{n,f}$ (kN)	$V_{n,p}/$ Peak load	$V_{n,ACI}$ (kN)			$V_{n,ACI}/$ Peak load
					Eq. (2.1)	$\frac{2}{3} \sqrt{f'_c} A_{cv}$	Limit	
WC150	870	1983	892	1.02	960	683	683	0.79
WD150	890	2193	975	1.09	1015	830	830	0.93
WD200	880	2045	909	1.03	813	759	759	0.85
WD170	980	2160	960	0.98	972	750	750	0.77
WCD170	890	2153	957	1.07	976	762	762	0.86
WD170A	1040	2451	1089	1.05	968	740	740	0.71

Table 3.1 Required lateral tie stiffness (Dhakal and Maekawa 2002)

Stable buckling mode, n th	Equivalent required stiffness, k _{eq} *	Required stiffness (kN/mm)	
		s = 60 mm, f _y = 574.9 MPa	s = 60 mm, f _y = 595.7 MPa
1	0.7500	130.4	132.8
2	0.1649	28.7	29.2
3	0.0976	17.0	17.3
4	0.0448	7.8	7.9
5	0.0084	1.5	1.5

*k_{eq} is the required lateral tie stiffness normalized with $\frac{\pi^4 EI}{s^3}$

where EI is average flexural rigidity of the main bar which equal to $0.5E_s I_s \sqrt{\frac{f_y}{400}}$

(MPa), s is a spacing of lateral ties

Table 3.2 Reinforcement properties (unit in MPa)

Specimen	Longitudinal reinforcement				Web reinforcement			
	f _y	f _u	ε [•]	σ [•]	f _y	f _u	ε [•]	σ [•]
WC150	574.9	646.8	0.0392	502.2	451.3	715.5	0.0158	295.6
WD150	574.9	646.8	0.0392	502.2	451.3	715.5	0.0158	295.6
WD170	595.7	664.0	0.0384	511.5	505.9	682.7	0.0177	263.2
WD200	574.9	646.8	0.0392	502.2	451.3	715.5	0.0158	210.5
WCD170	595.7	664.0	0.0384	511.5	505.9	682.7	0.0177	263.2
WD170A	595.7	664.0	0.0384	511.5	505.9	682.7	0.0177	263.2

Table 3.3 Buckling strength of web bars

Specimen	WC150, WD150	WD200	WD170, WCD170, WD170A
Yield strength of web bar (MPa)	451.3	451.3	505.9
Spacing (s, mm)	150	200	170
Radius of gyration (r, mm)	2.50	2.50	2.50
Elastic modulus (E, MPa)	200000	200000	200000
Elastic buckling stress $\left(\frac{\pi^2 E}{\left(\frac{s}{r} \right)^2} \right) (\text{MPa})$	548.3	308.4	426.9
Elastic buckling strain (ε_b)	0.00226	0.00154	0.00213

Table 3.4 Concrete properties (unit in MPa)

Specimen	Unconfined concrete (used for web elements)			Confined concrete including buckling and concrete cover spalling effect (used for boundary column elements)		
	f'_c	ε_0	ε_{85}	f'_c	ε_0	ε_{85}
WC150	27.3	0.002	0.0038	31.1	0.0047	0.0120
WD150	40.3	0.002	0.0038	44.1	0.0039	0.0108
WD170	32.9	0.002	0.0038	36.9	0.0044	0.0113
WD200	33.7	0.002	0.0038	37.5	0.0043	0.0112
WCD170	33.9	0.002	0.0038	37.9	0.0044	0.0113
WD170A	32.4	0.002	0.0038	36.3	0.0045	0.0115

FIGURES

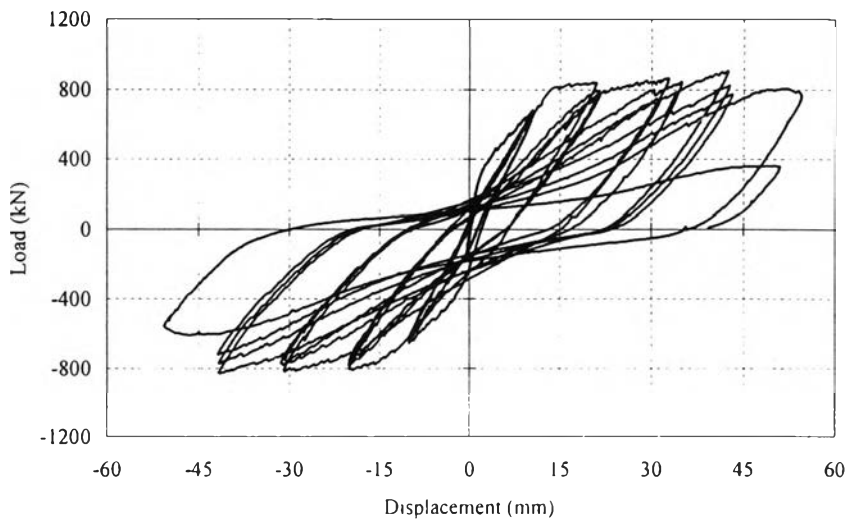


Fig. 1.1 Example of relationship between lateral load and lateral displacement

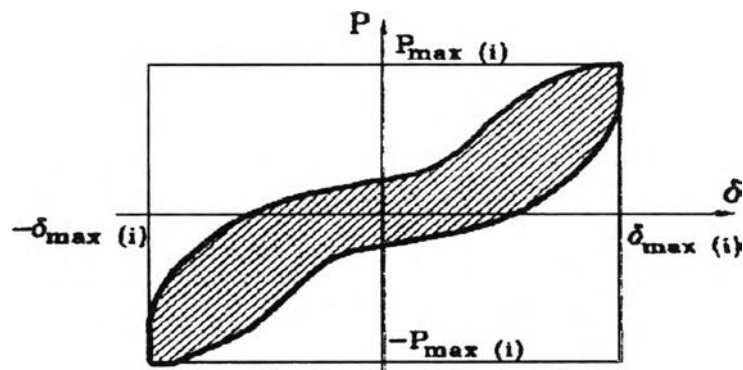


Fig. 1.2 Energy dissipation in one cycle (Hidelgo and Jordan 1996)

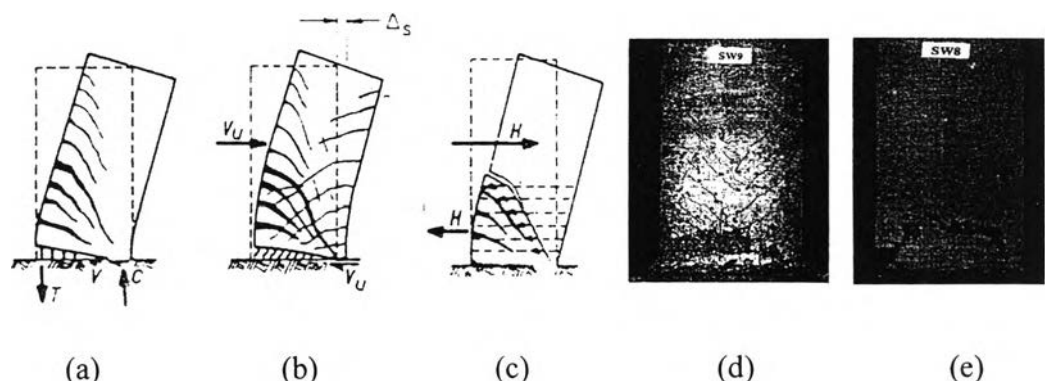


Fig. 1.3 Failure characteristics: (a) flexural failure; (b) shear sliding failure; (c) diagonal tension failure; (d) web crushing failure; (e) out-of-plane buckling failure
(Ref.: (a)-(c) from Paulay et al. (1980), (d)-(e) from Zhang and Wang (2000))

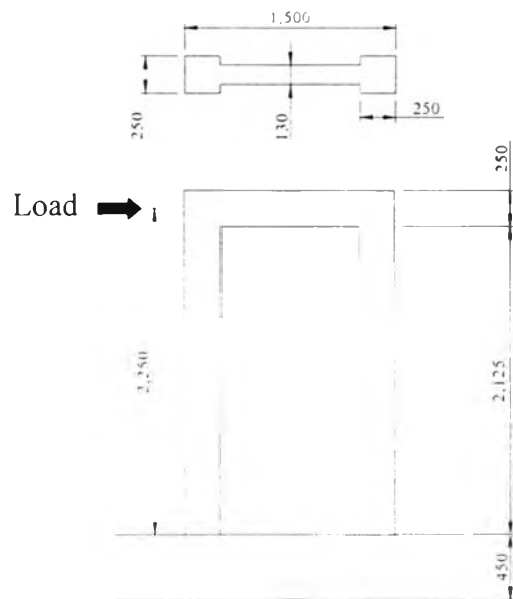


Fig.2.1 Dimensions of specimens (dimensions in mm)

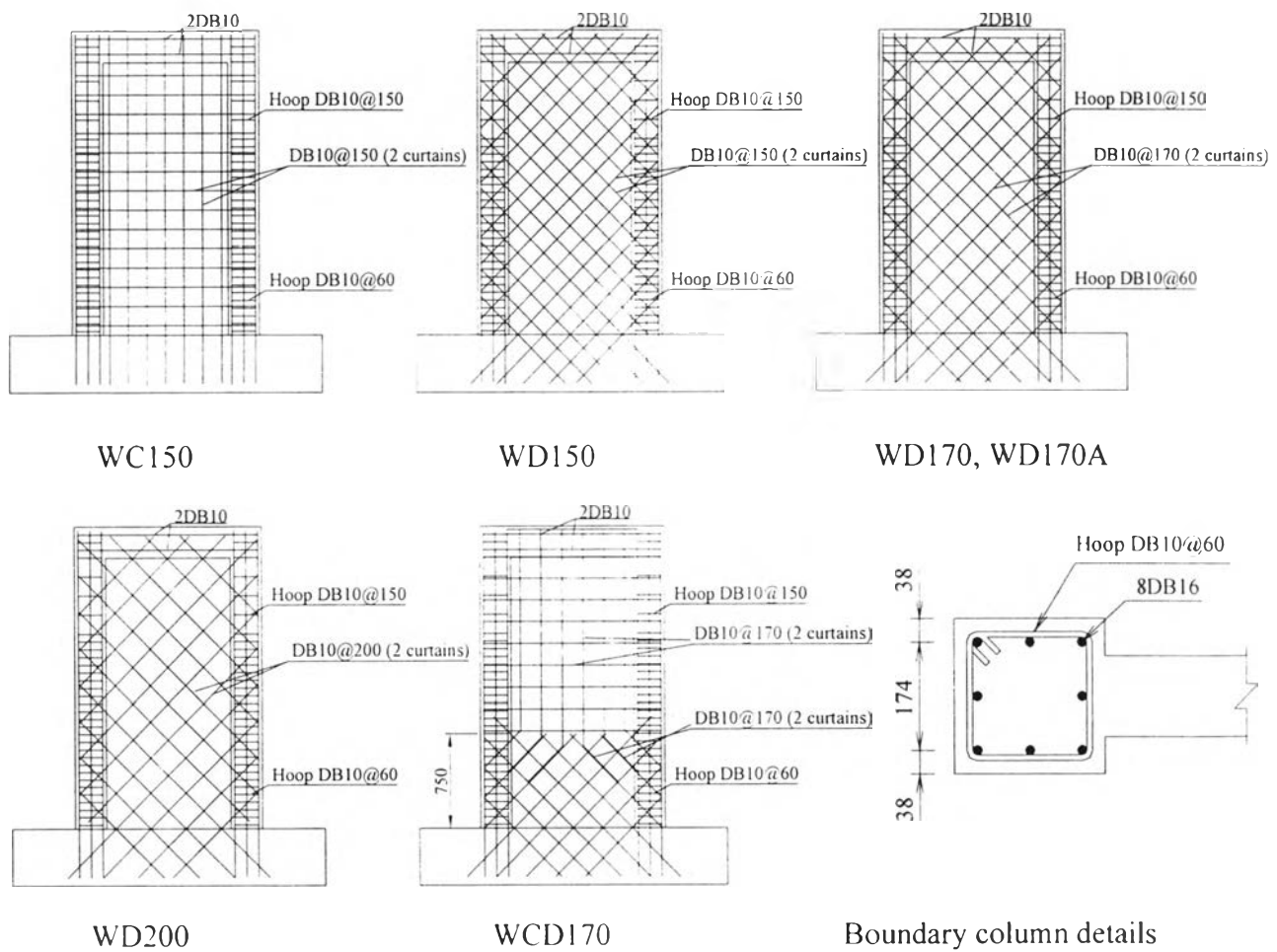


Fig.2.2 Reinforcement details (dimensions in mm)

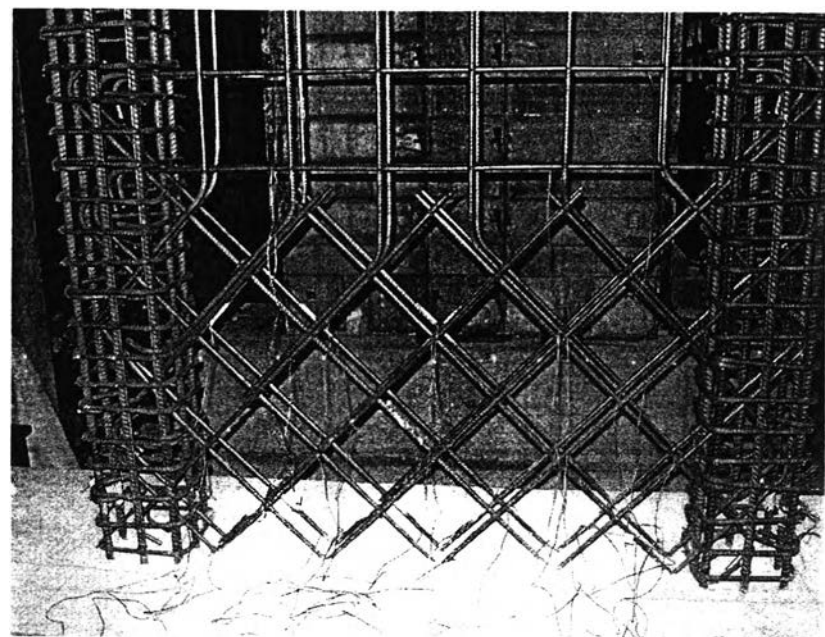


Fig.2.3 Splice detail of specimen WCD170

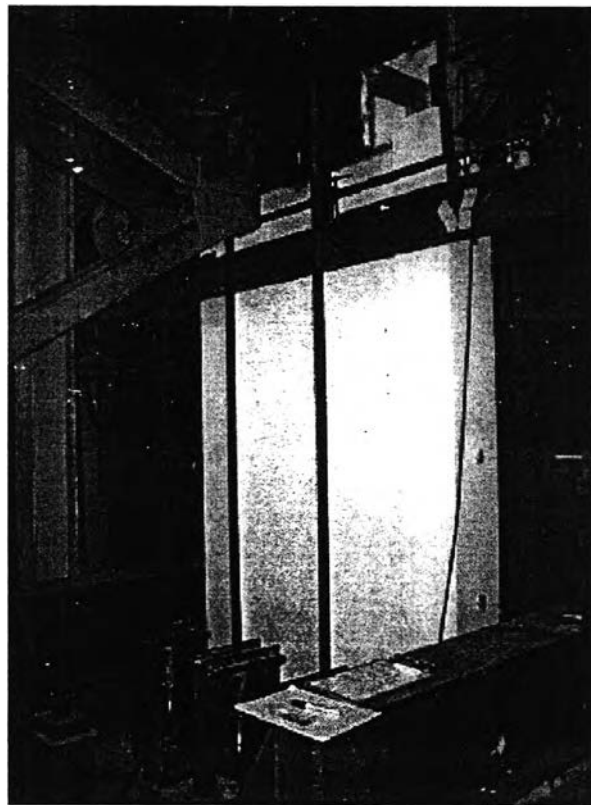


Fig.2.4 Overview of test setup

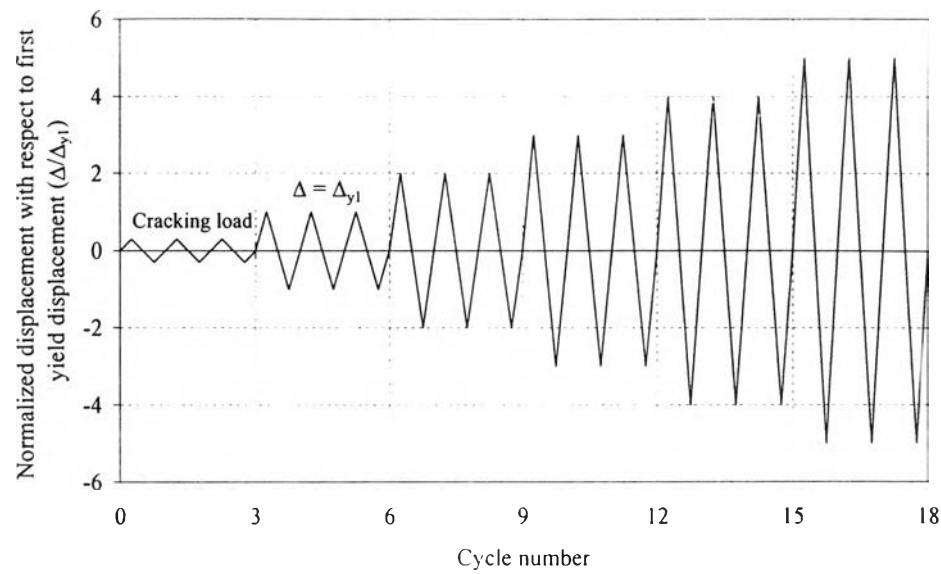


Fig.2.5 Displacement history

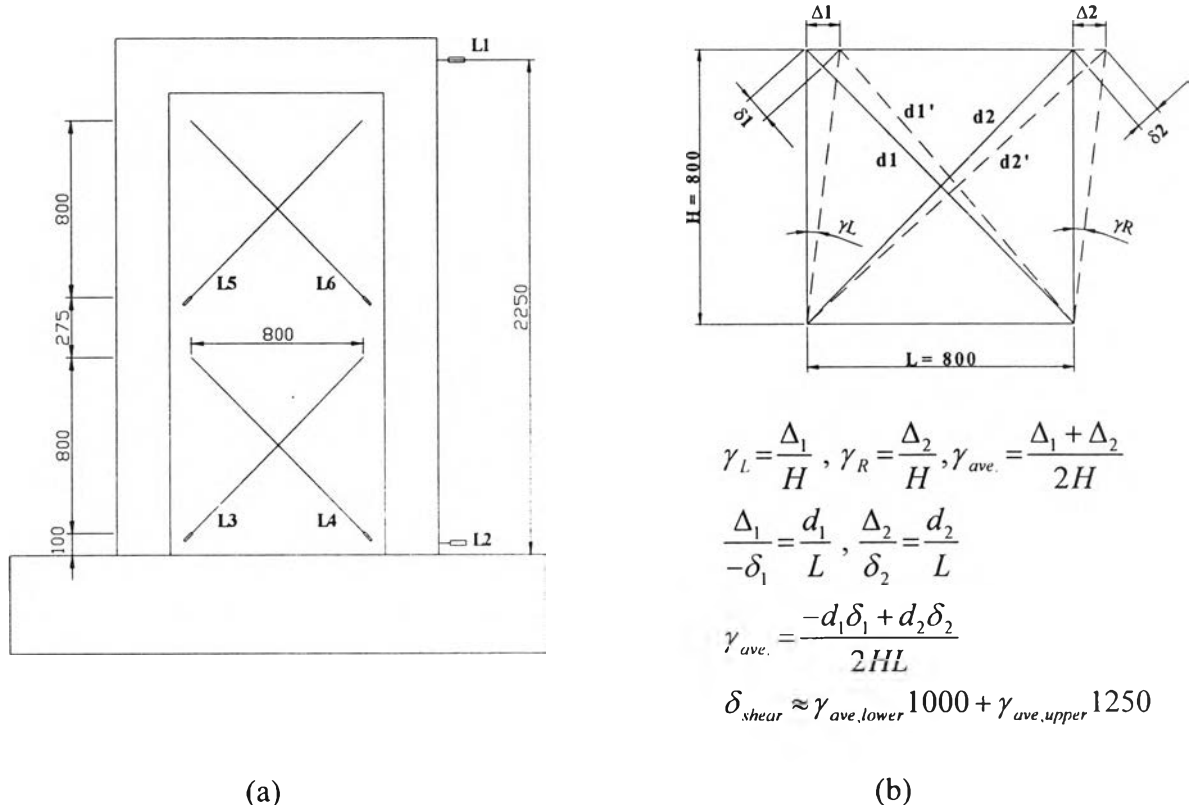


Fig.2.6 (a) Positions of LVDT's ; (b) Average shear displacement computation

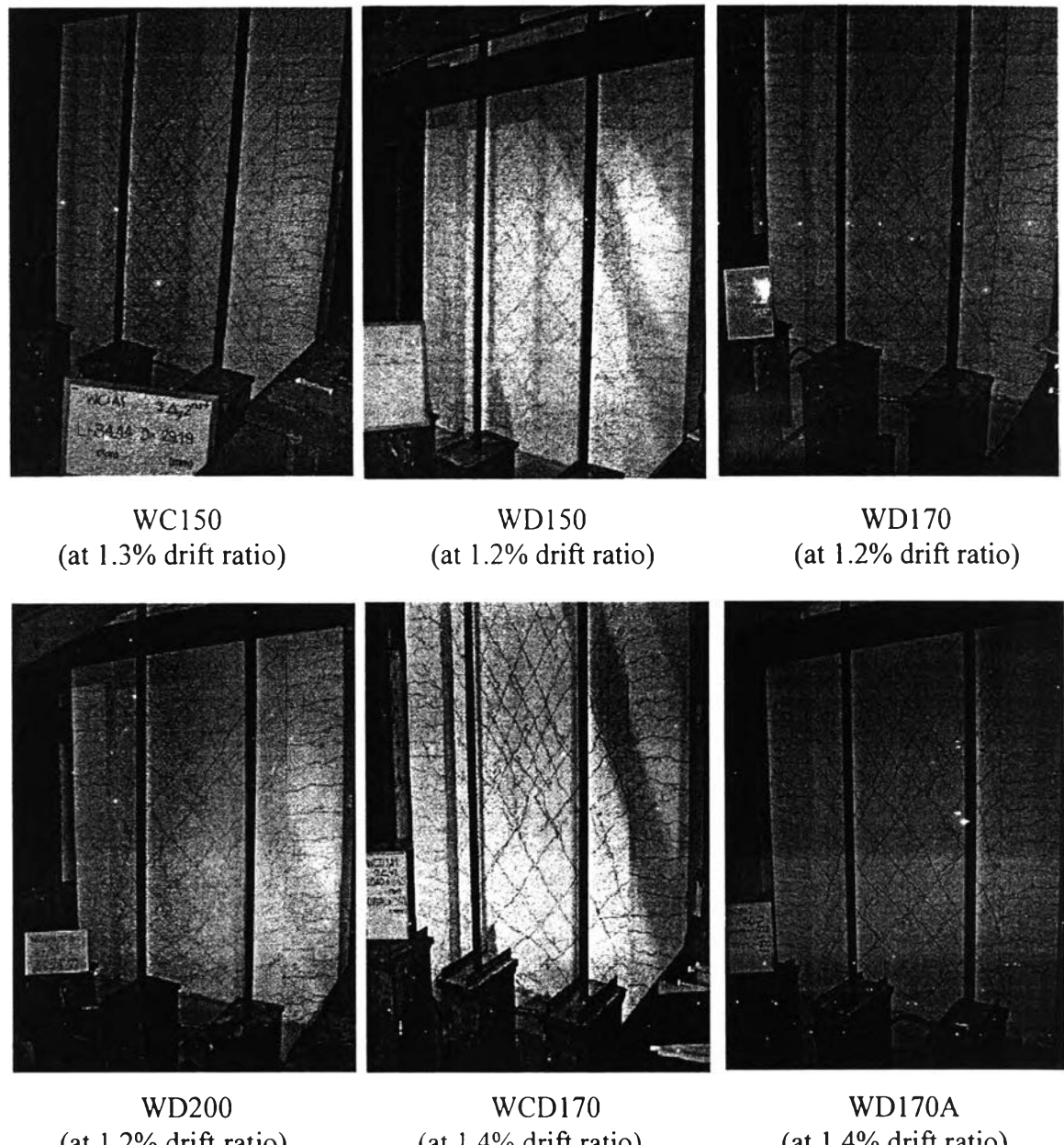


Fig.2.7 Comparison of crack patterns of wall specimens at approximately the same drift level: (a) WC150; (b) WD150; (c) WD170; (d) WD200; (e) WCD170; (f) WD170A

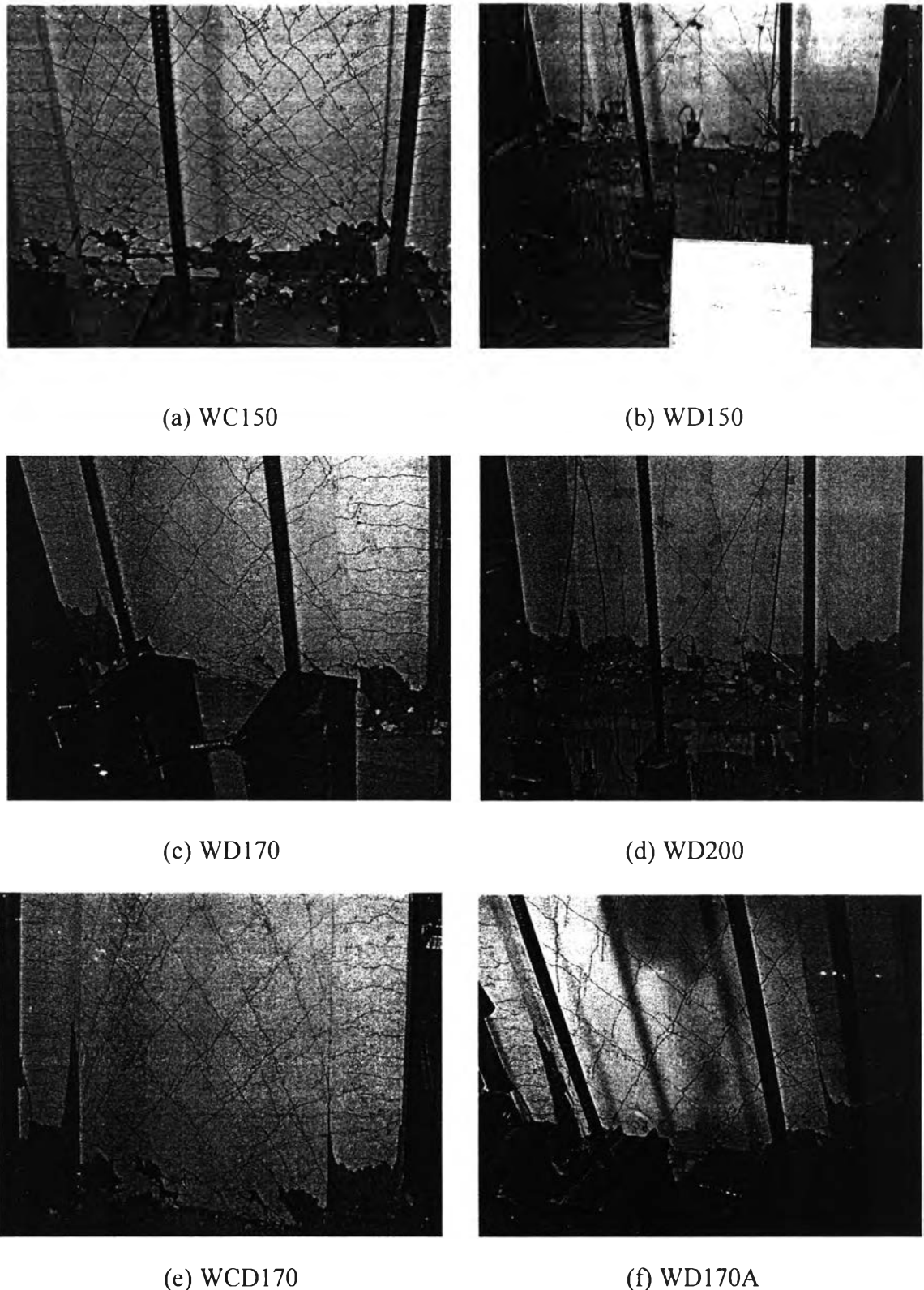


Fig.2.8 Wall specimens at failure

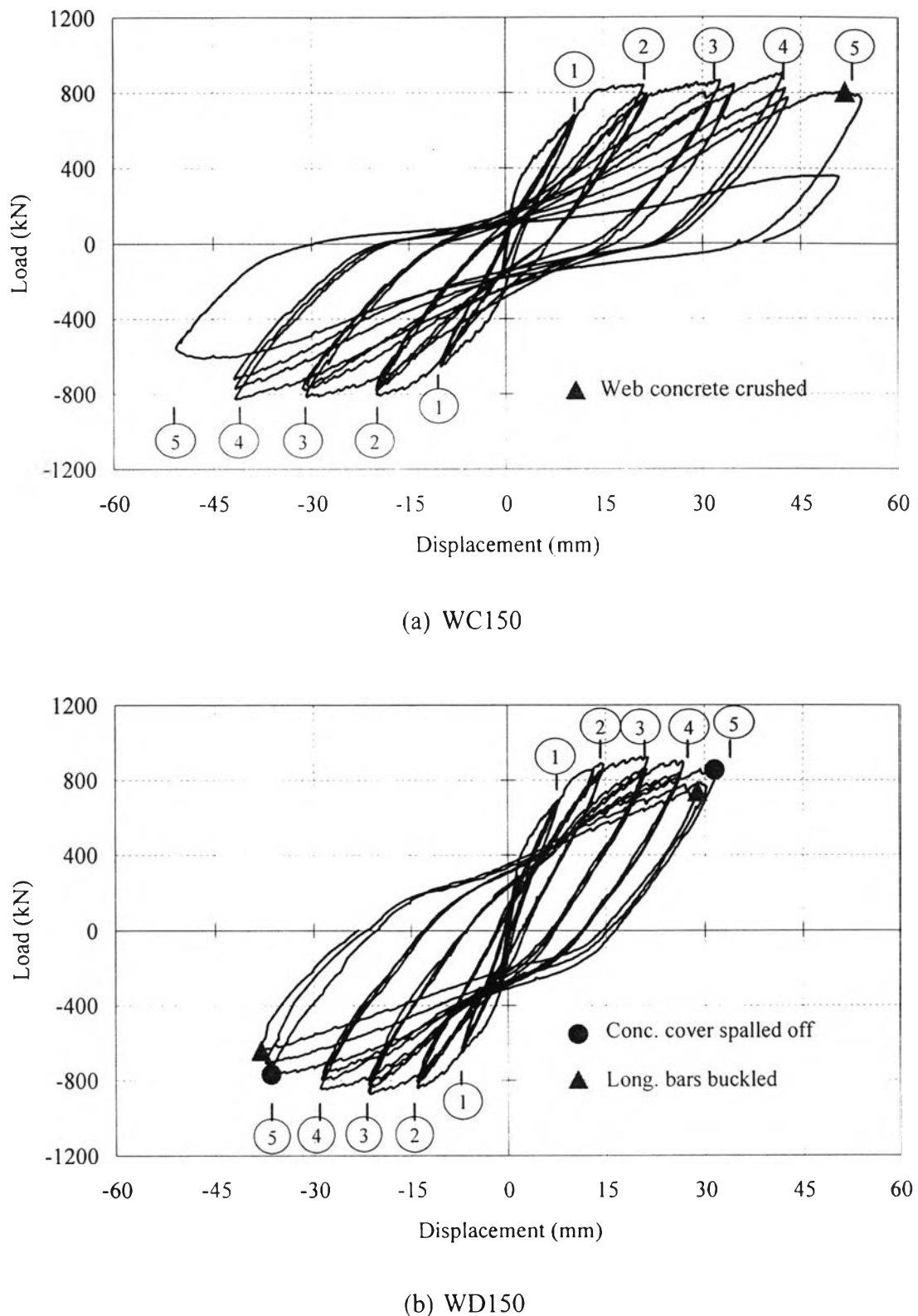
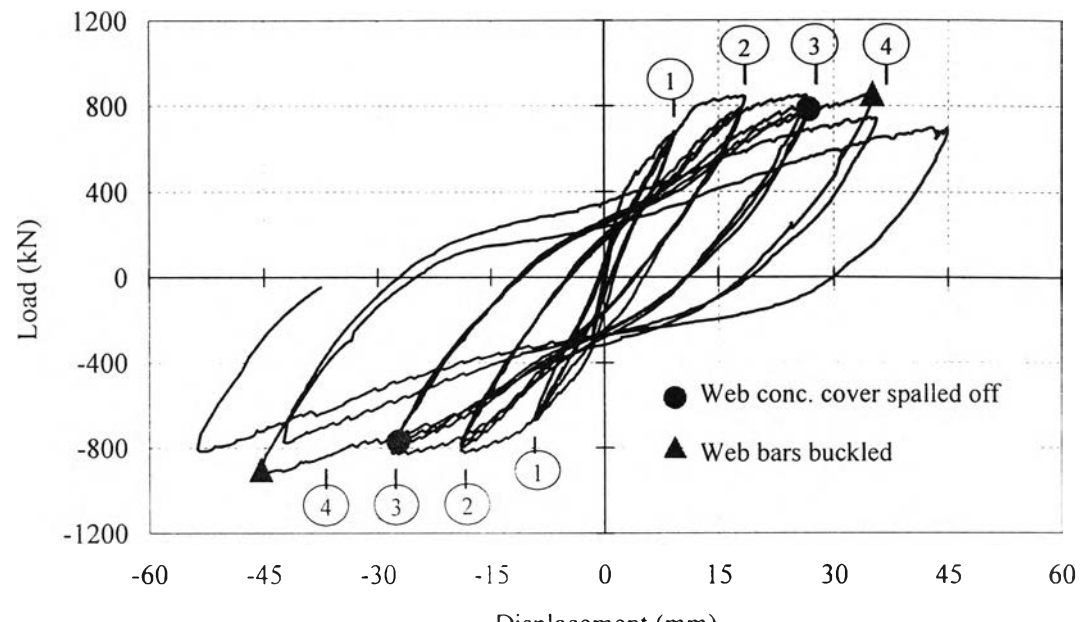
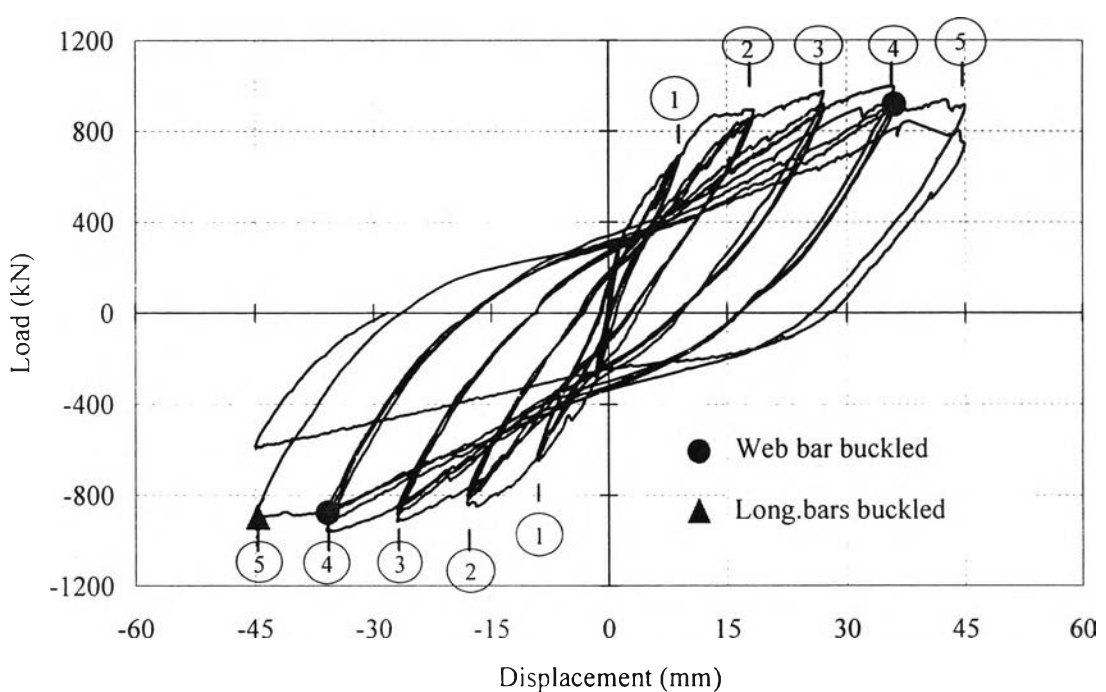


Fig. 2.9 Load-displacement hysteresis: (a) WC150; (b) WD150

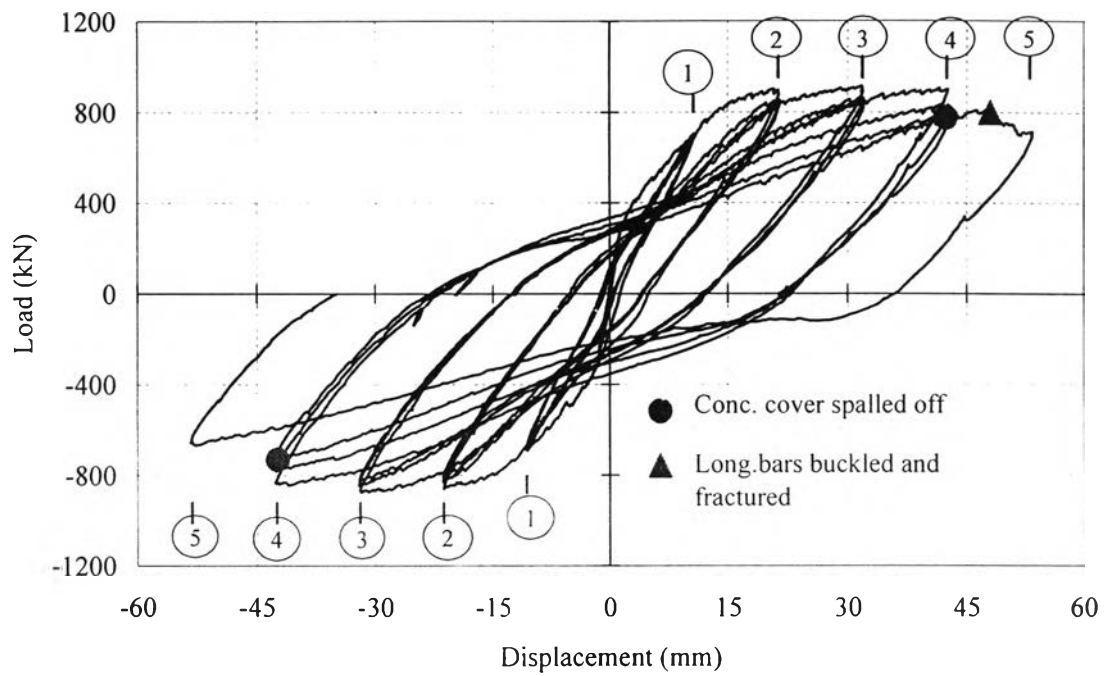


(c) WD200

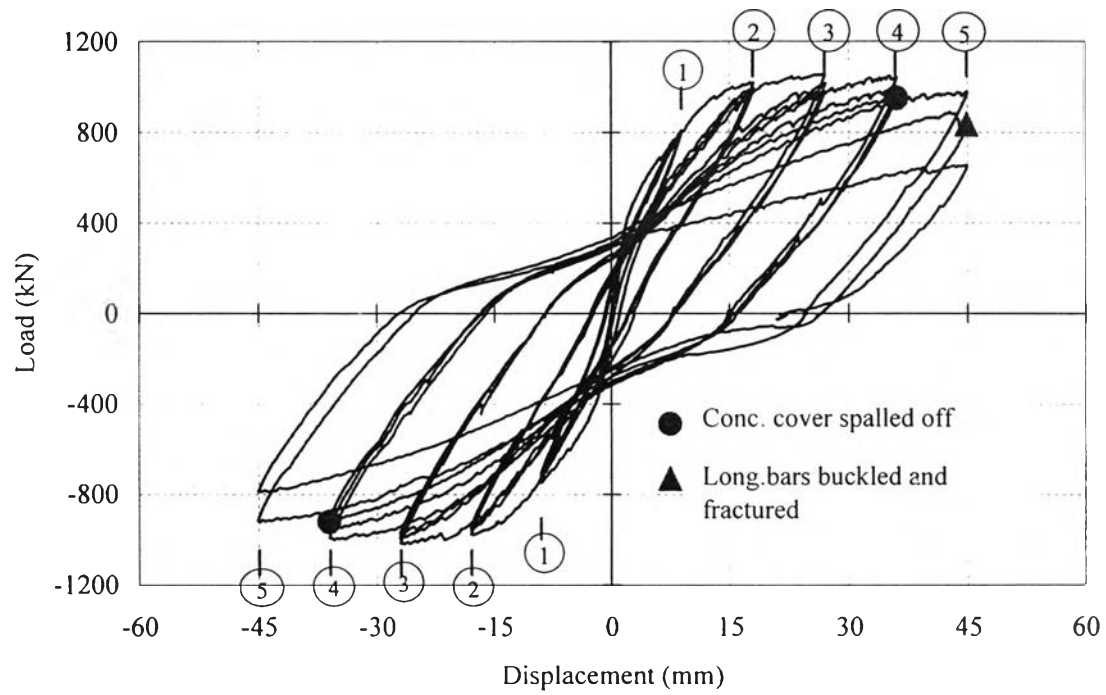


(d) WD170

Fig. 2.9 Load-displacement hysteresis (continue): (c) WD200; (d) WD170



(e) WCD170



(f) WD170A

Fig. 2.9 Load-displacement hysteresis (continue): (e) WCD170; (f) WD170A

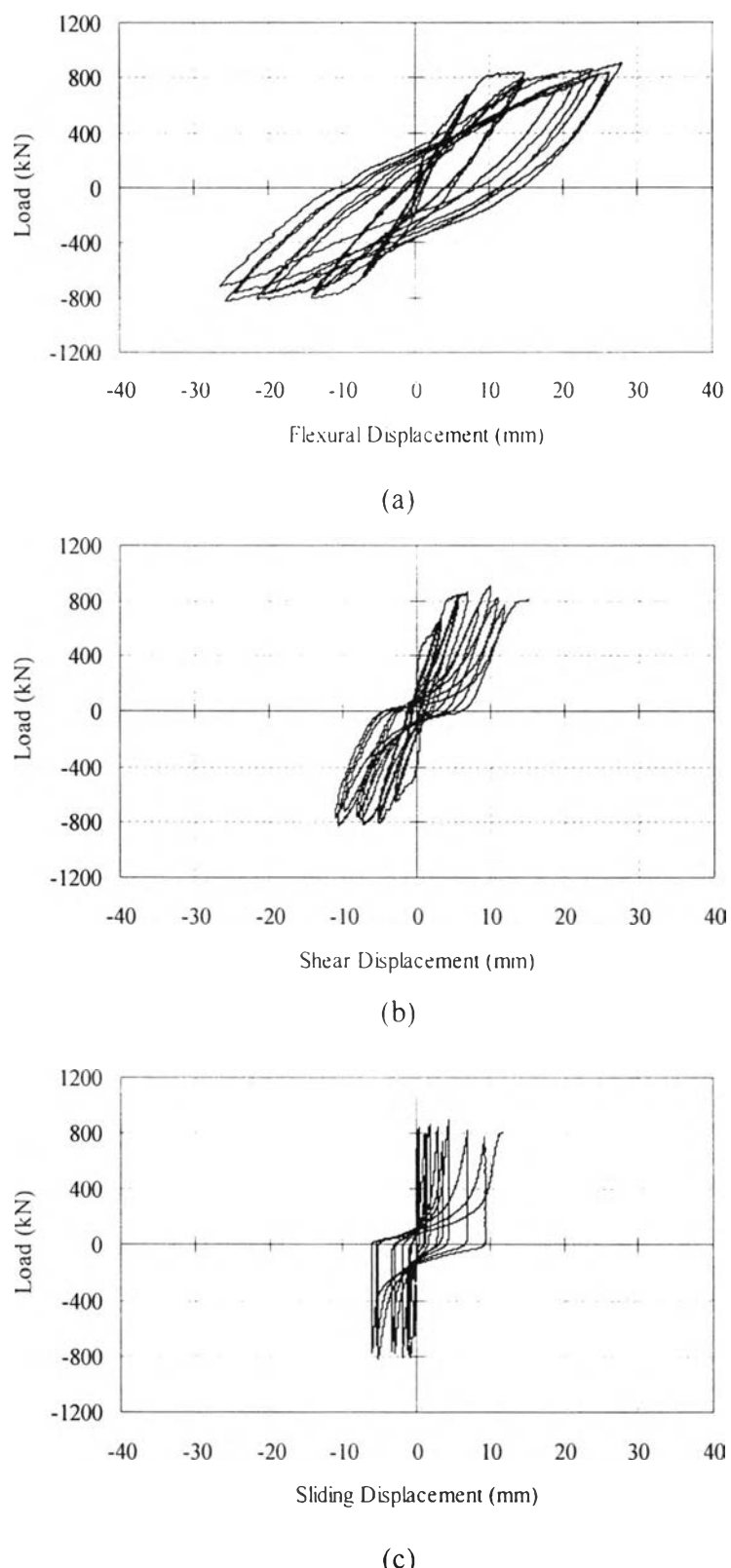


Fig. 2.10(a) Displacement components of specimen WC150:

(a) flexural displacement; (b) shear displacement; (c) sliding displacement

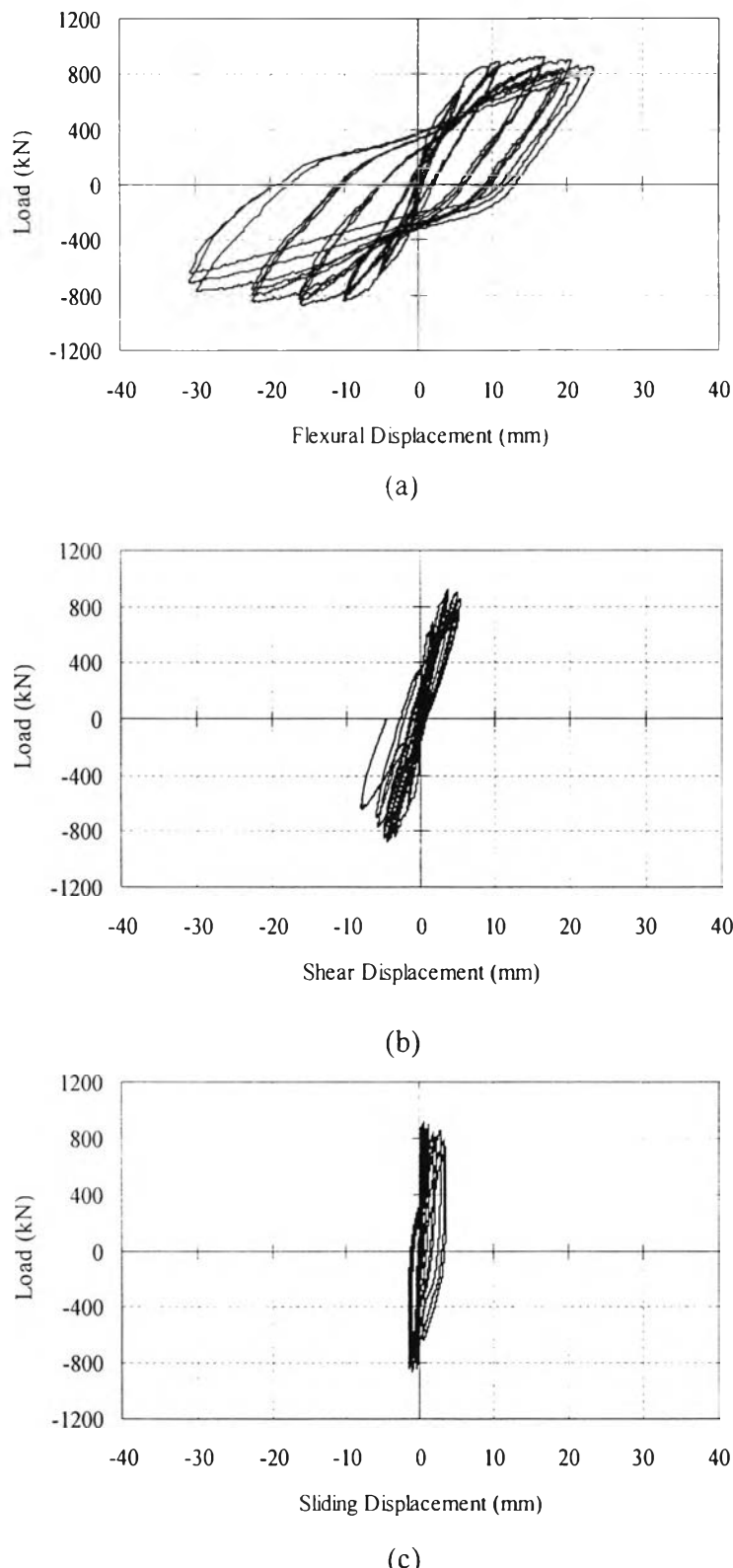


Fig. 2.10(b) Displacement components of specimen WD150:

(a) flexural displacement; (b) shear displacement; (c) sliding displacement

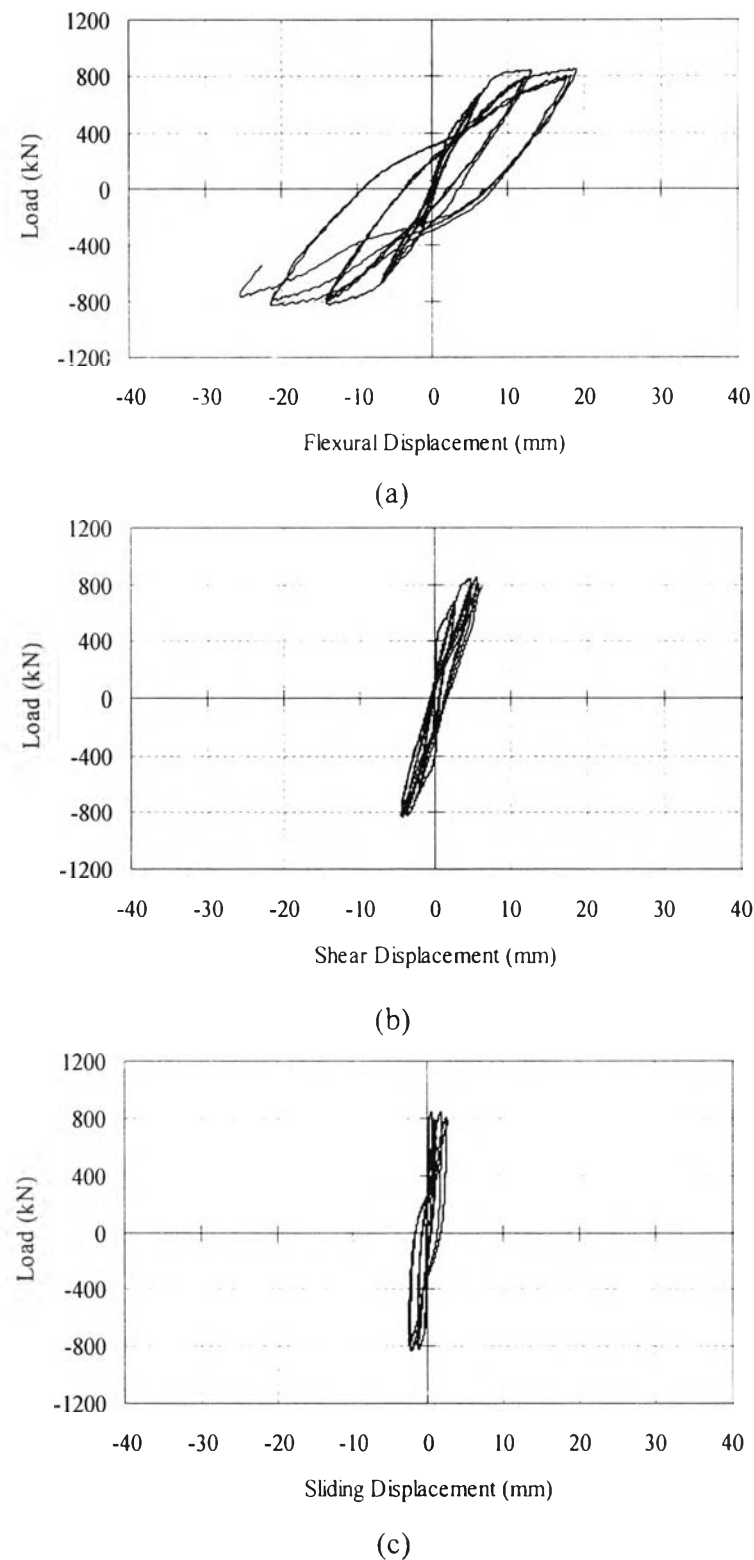


Fig. 2.10(c) Displacement components of specimen WD200:
 (a) flexural displacement, (b) shear displacement, (c) sliding displacement

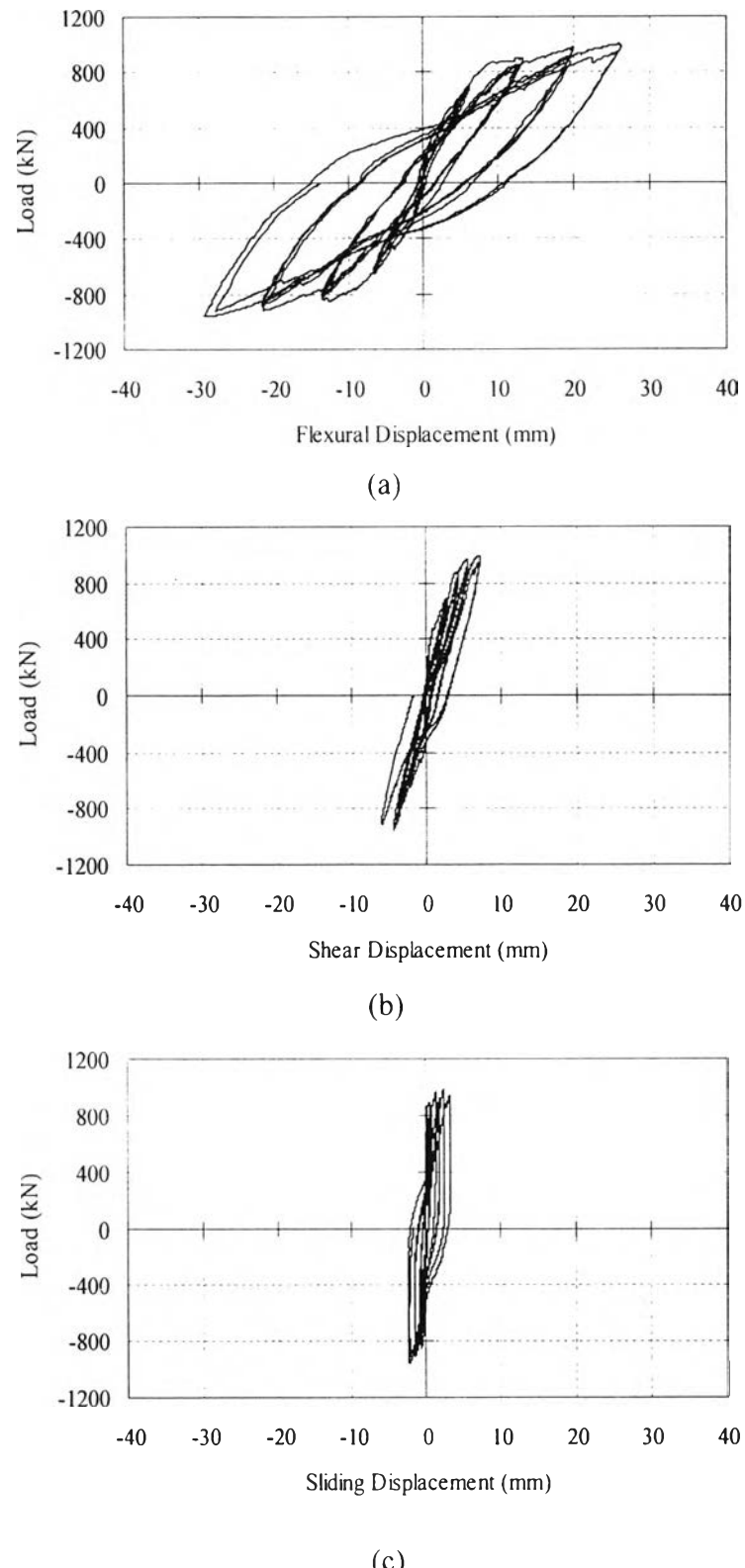


Fig. 2.10(d) Displacement components of specimen WD170:

(a) flexural displacement; (b) shear displacement; (c) sliding displacement

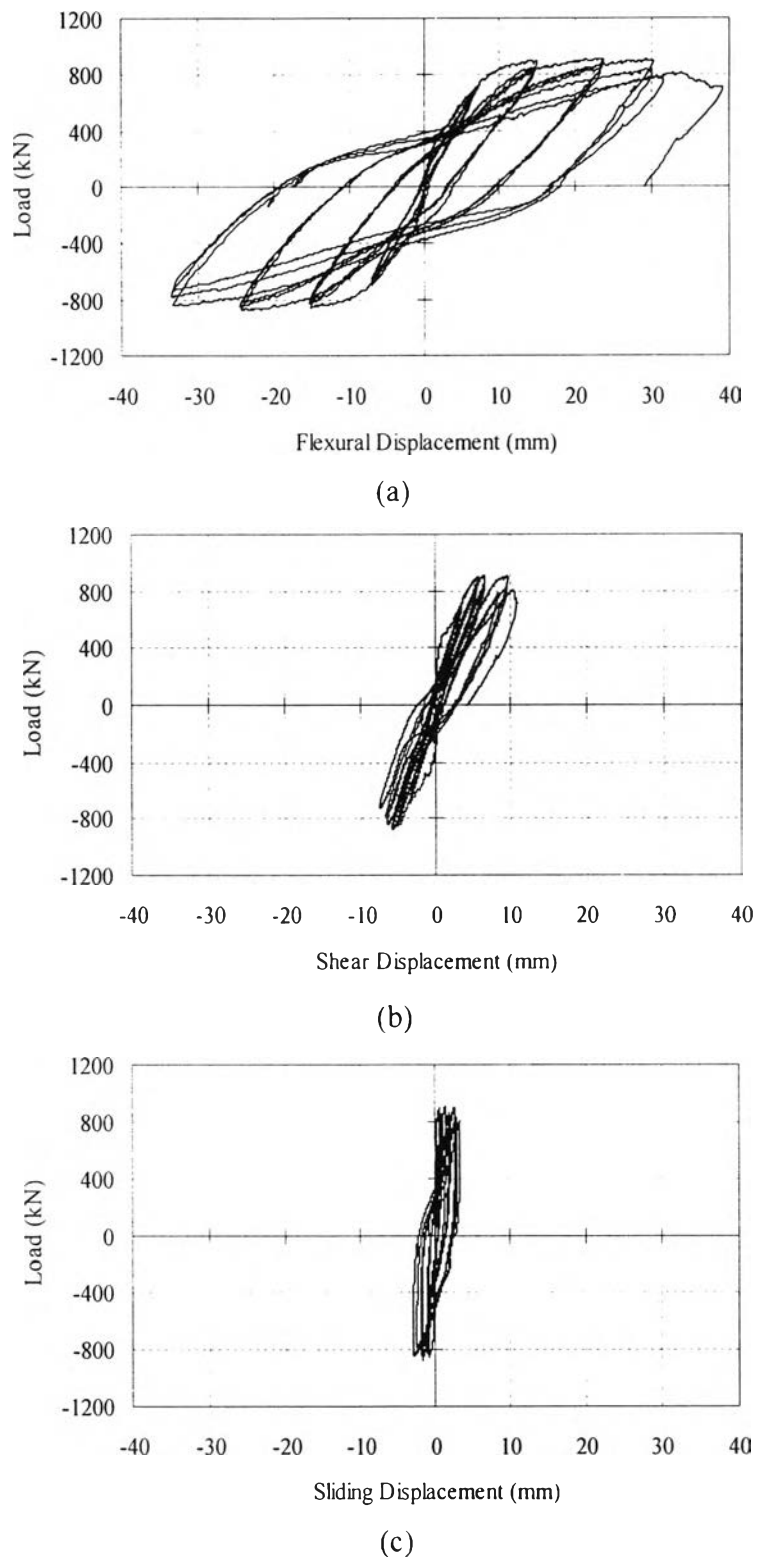


Fig. 2.10(e) Displacement components of specimen WCD170:
 (a) flexural displacement; (b) shear displacement; (c) sliding displacement

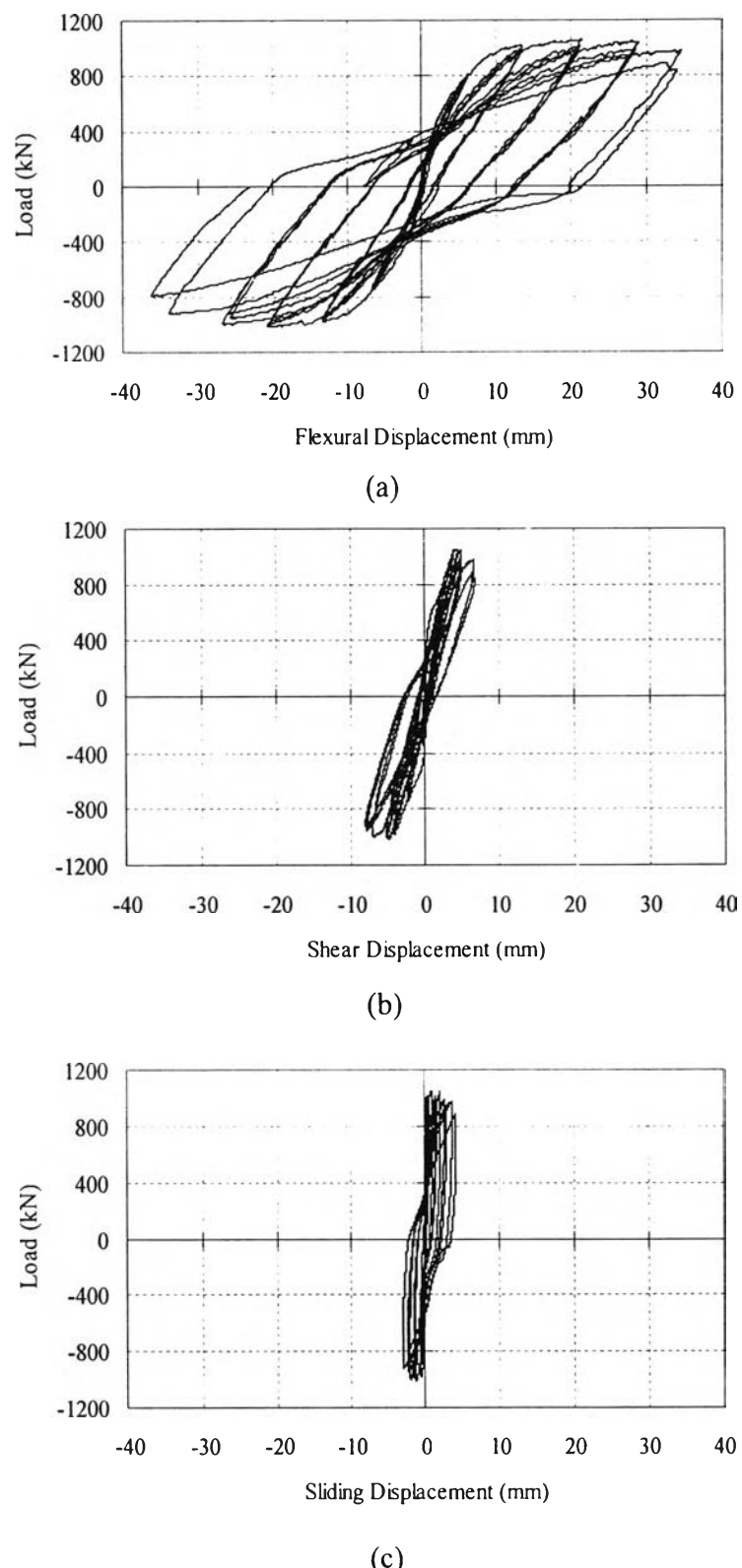


Fig. 2.10(f) Displacement components of specimen WD170A:
 (a) flexural displacement; (b) shear displacement; (c) sliding displacement

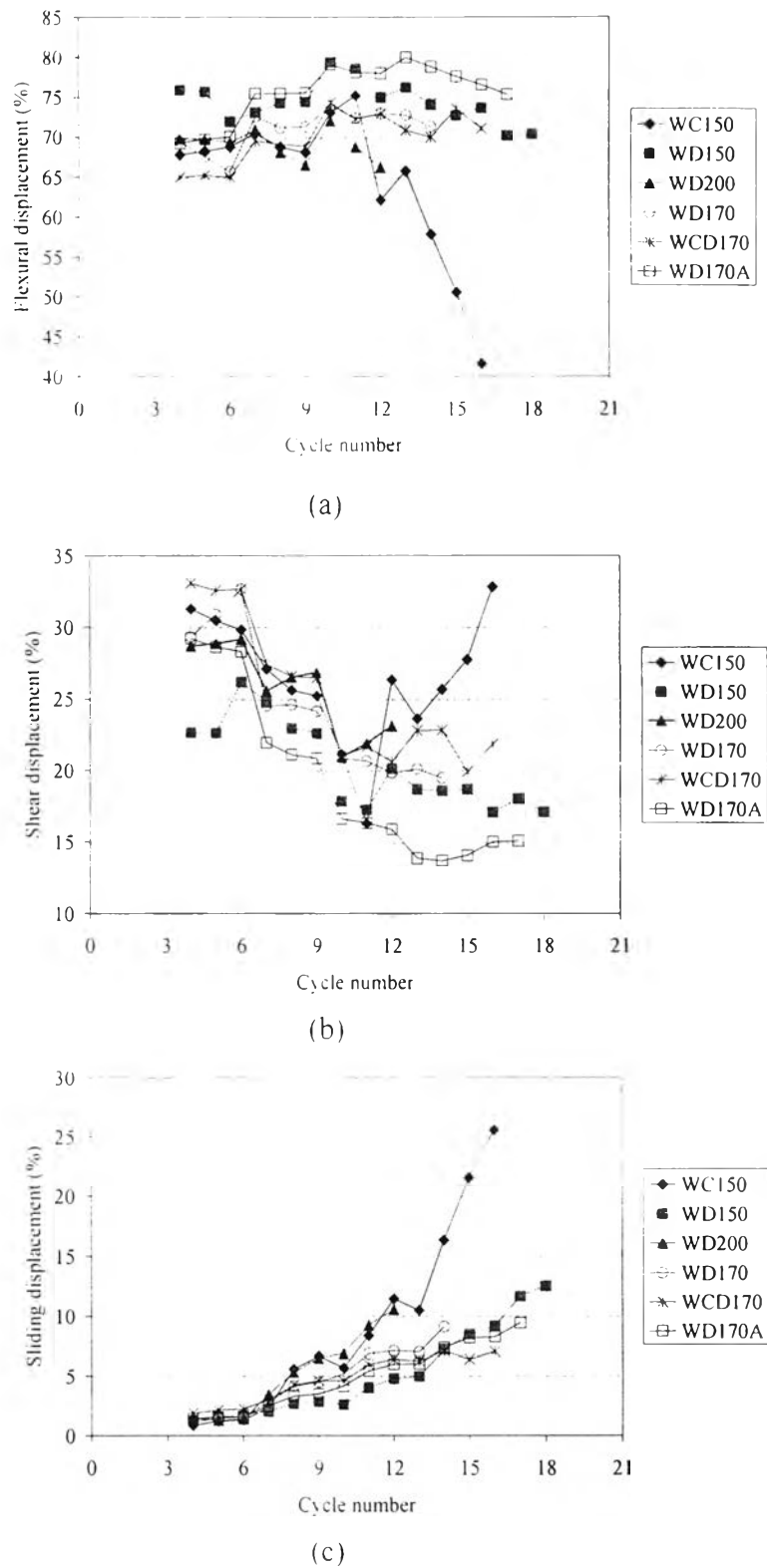


Fig. 2.11 Displacement components as percentage of total displacement:
 (a) flexural displacement; (b) shear displacement; (c) sliding displacement

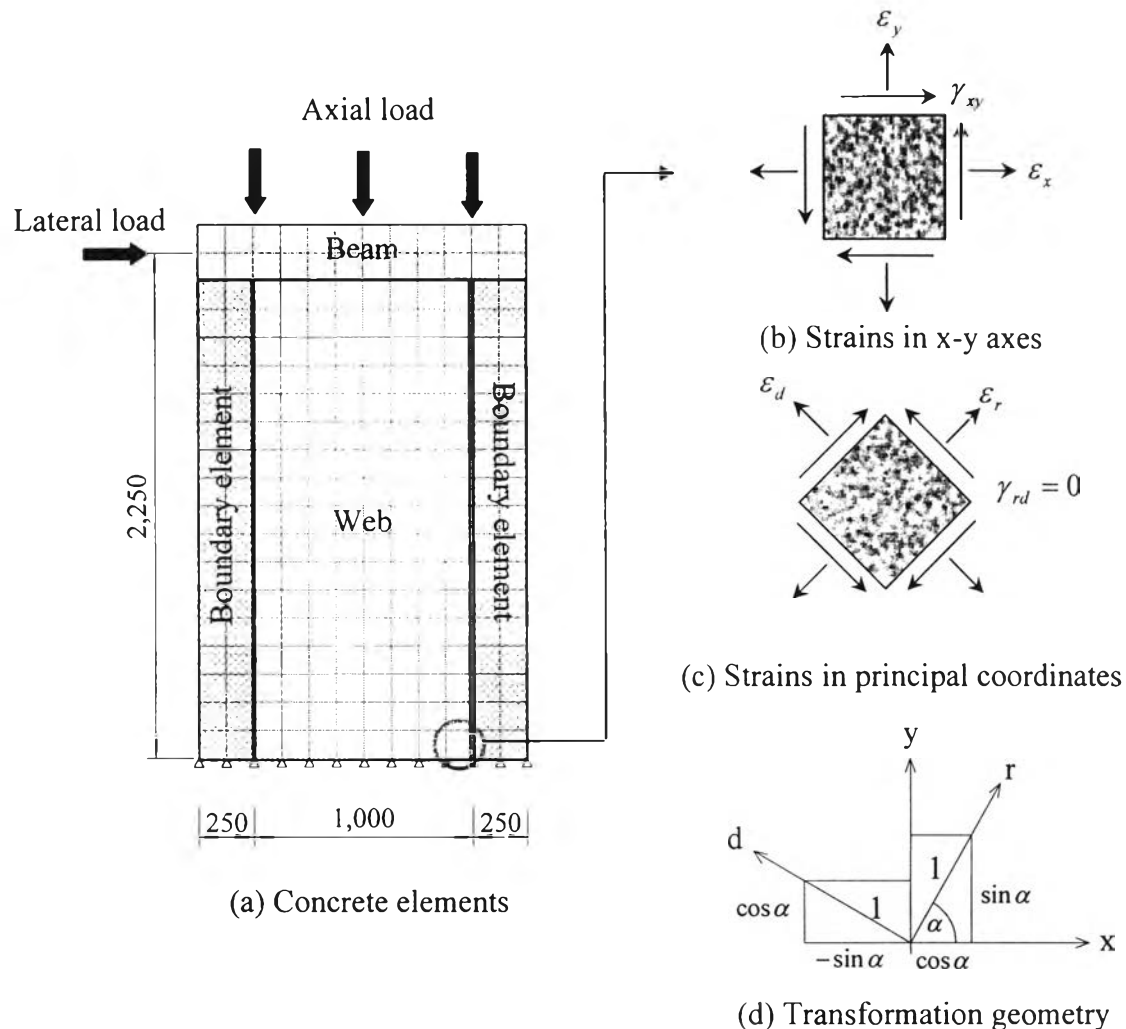


Fig.2.12 Transformation of strains in concrete at the base and adjacent to the boundary element

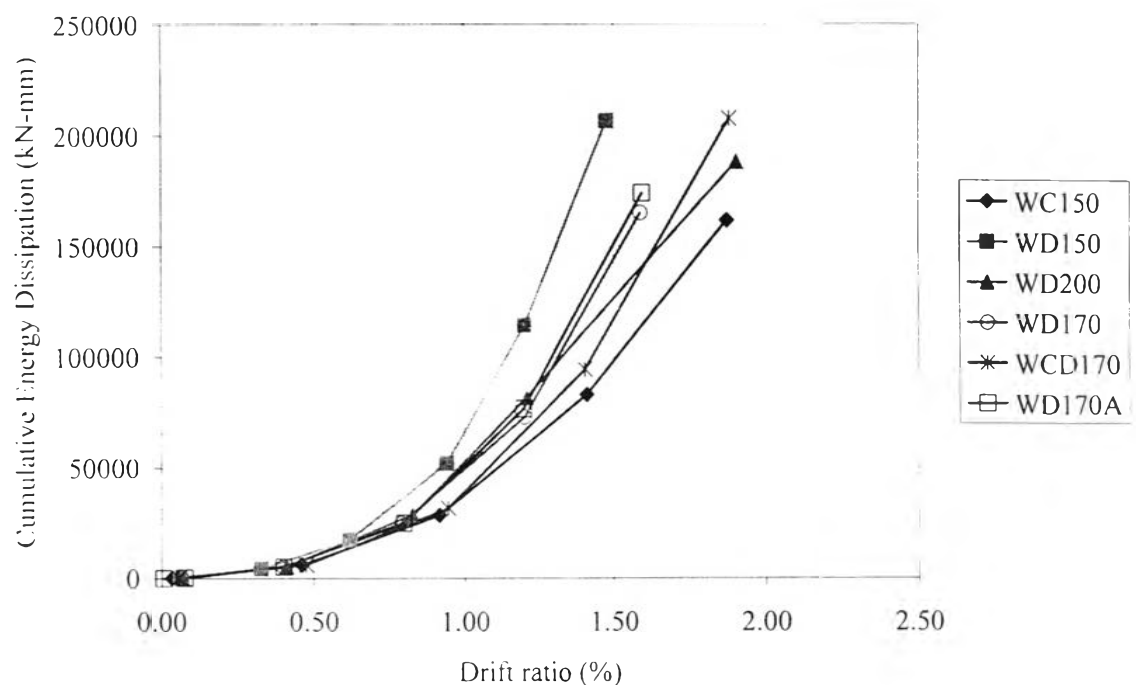


Fig. 2.13 Energy dissipation

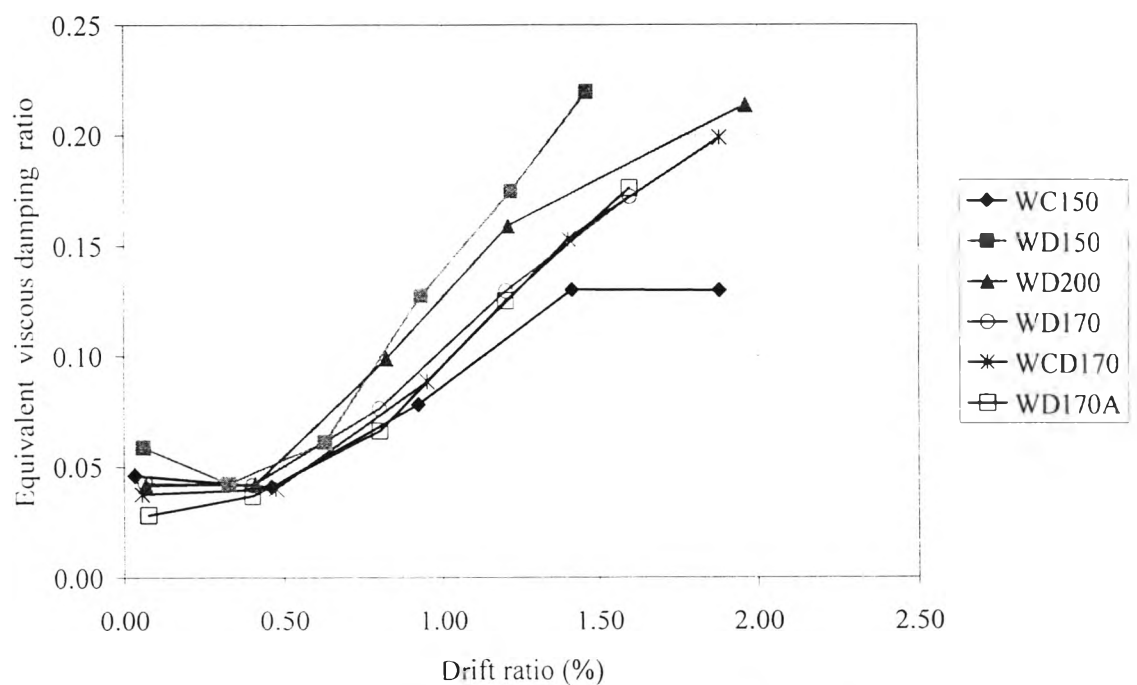


Fig. 2.14 Equivalent viscous damping ratio

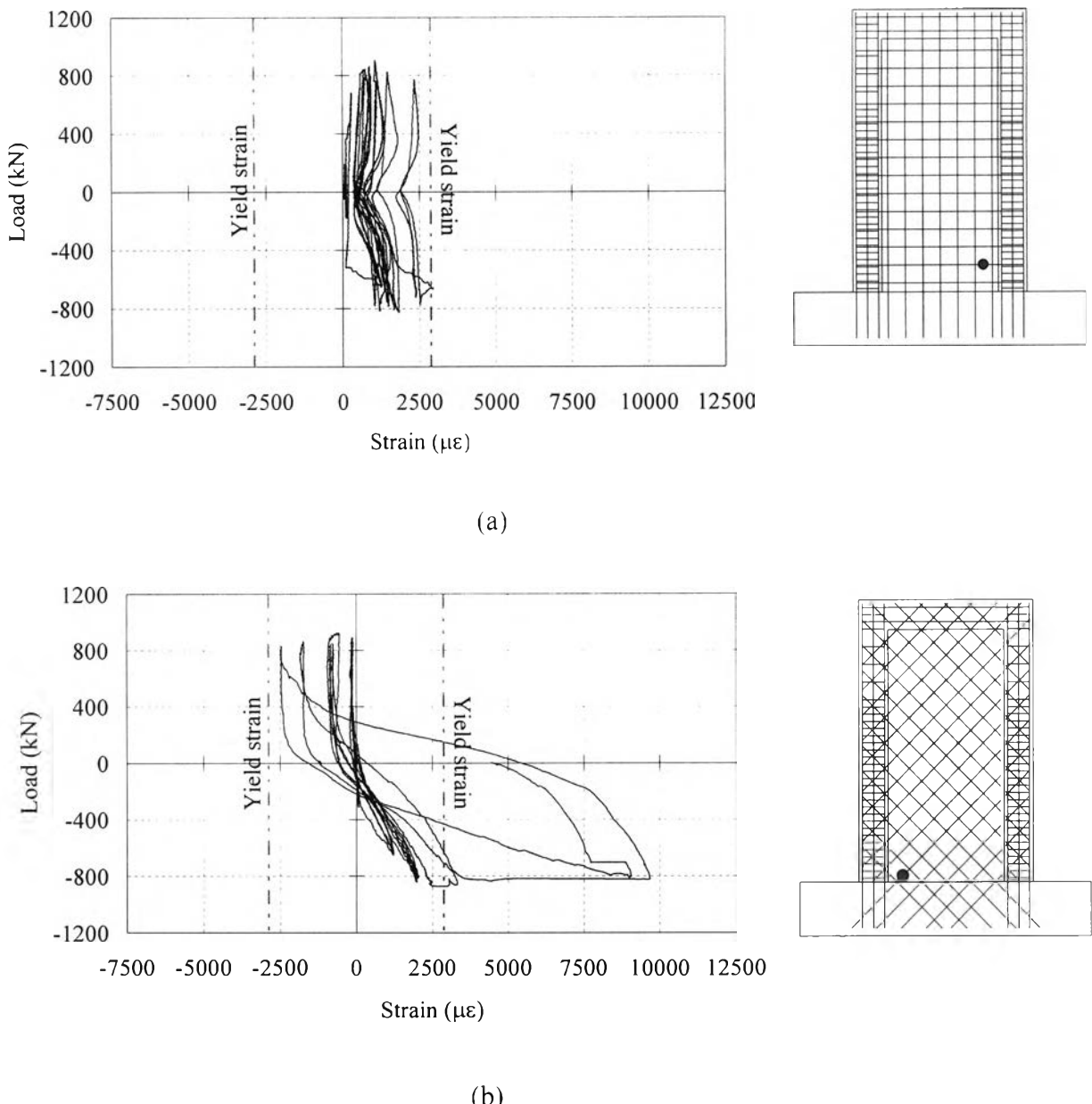


Fig. 2.15 Strain responses of web reinforcement:

(a) horizontal reinforcement in WC150; (b) diagonal reinforcement in WD150

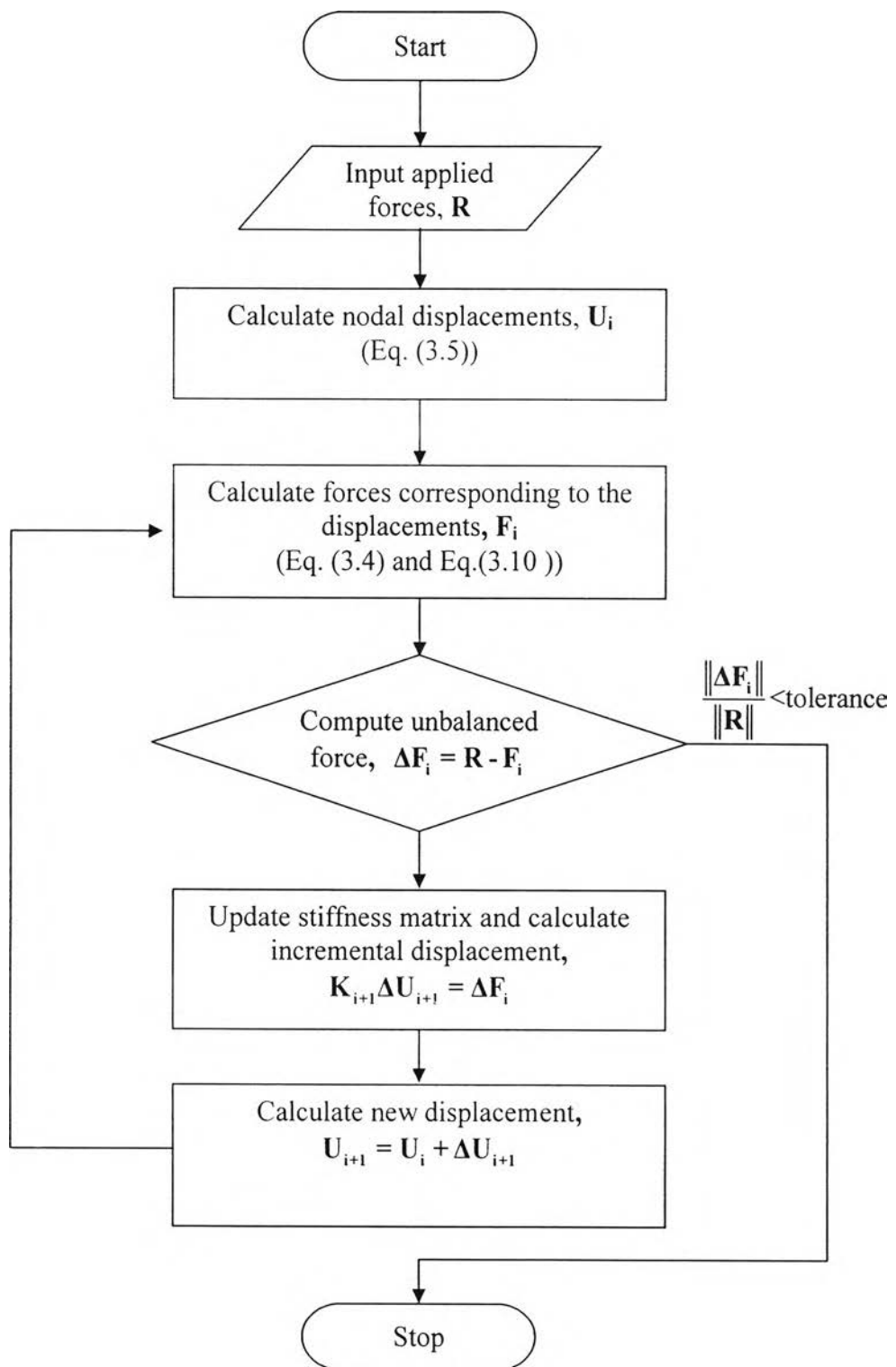


Fig. 3.1 Nonlinear analysis algorithm

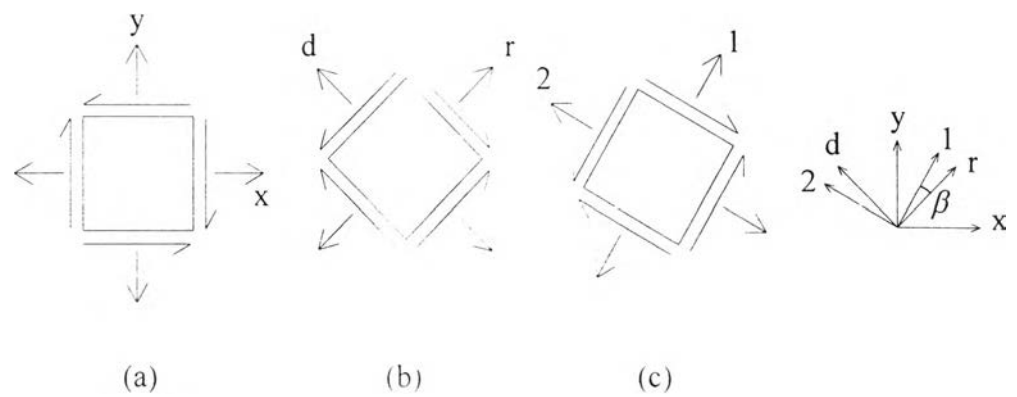
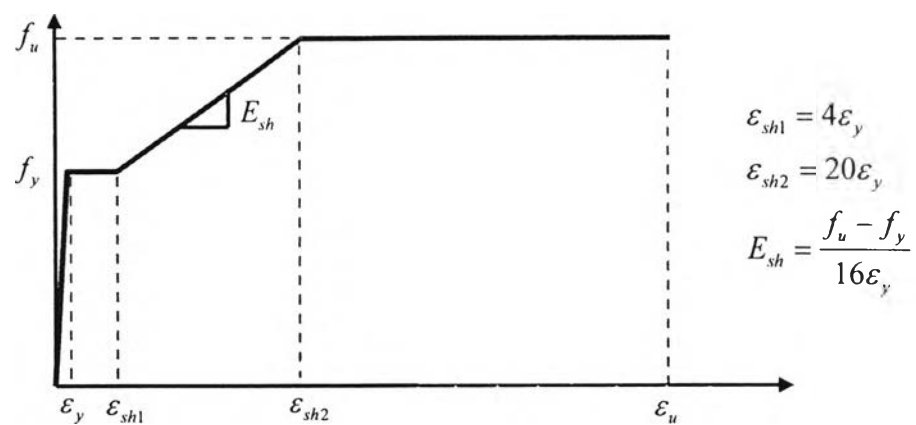
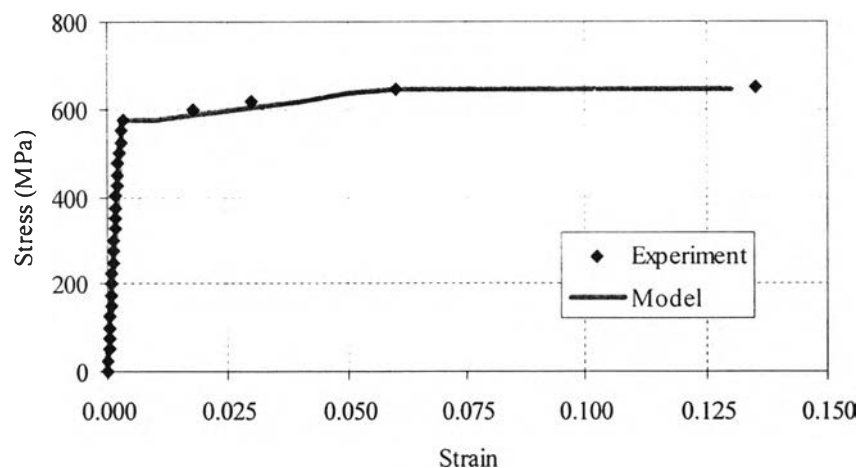


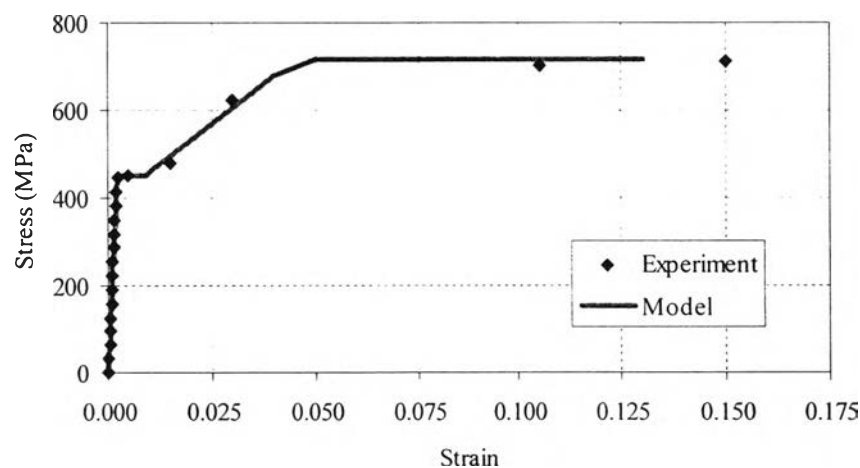
Fig. 3.2 (a) Global directions; (b) Principal directions; (c) Crack directions



(a) Stress-strain model of reinforcing steel in tension

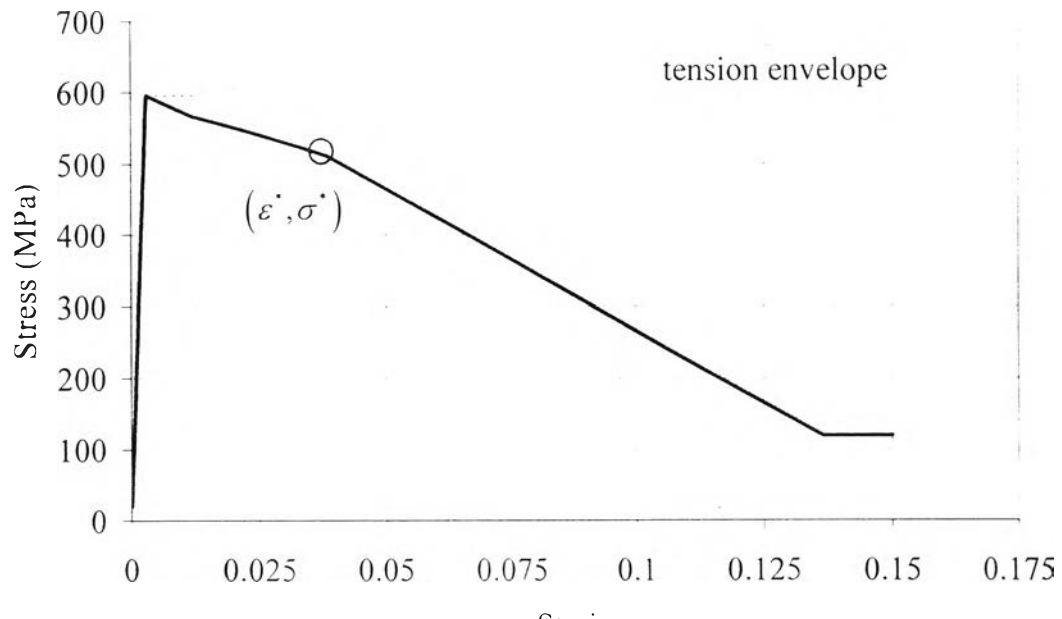


(b) Stress-strain relationship of longitudinal bars used in specimens WC150, WD150, and WD200

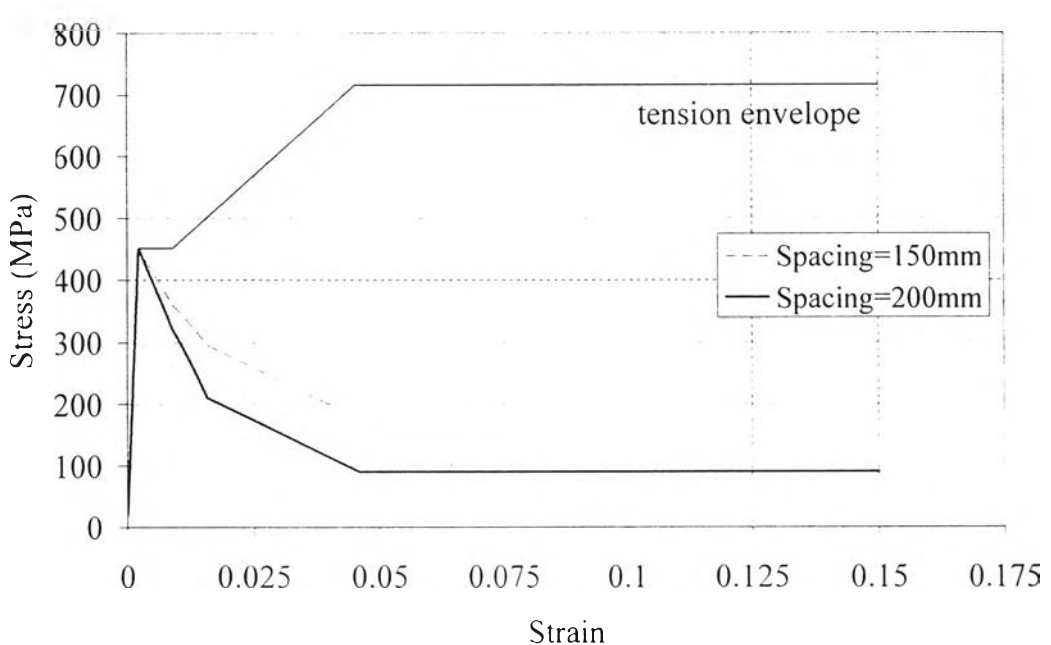


(c) Stress-strain relationship of web bars used in specimens WC150, WD150, and WD200

Fig. 3.3 Stress-strain relationships of reinforcing bars in tension



(a) Longitudinal bars of specimens WC150, WD150, and WD200



(b) Web bars of specimens WC150, WD150, and WD200

Fig. 3.4 Stress-strain relationships of reinforcing bars in compression
(Dhakal and Maekawa model)

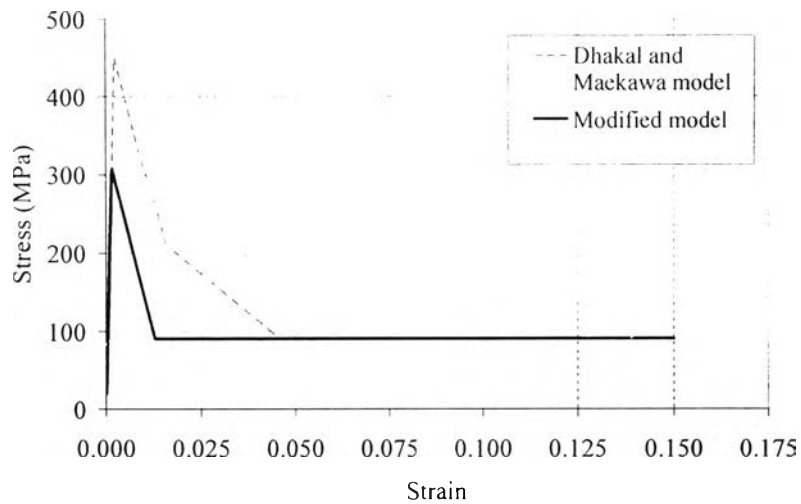


Fig. 3.5 Modified Dhakal and Maekawa model for web bars with elastic buckling of specimen WD200

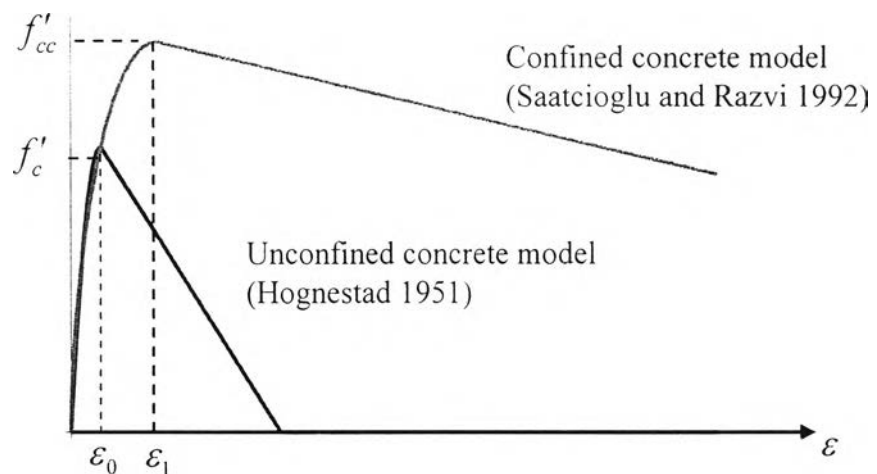


Fig. 3.6 Unconfined and confined concrete models

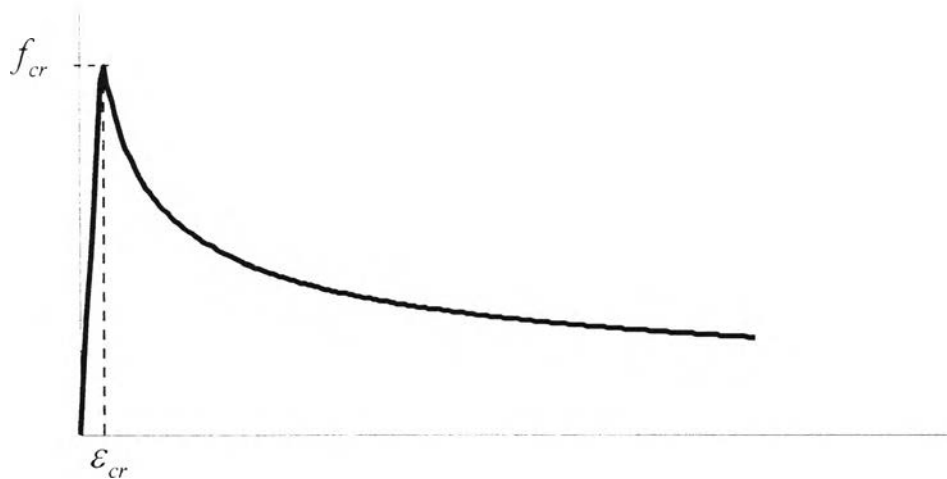


Fig. 3.7 Concrete model in tension (Belarbi and Hsu 1994)

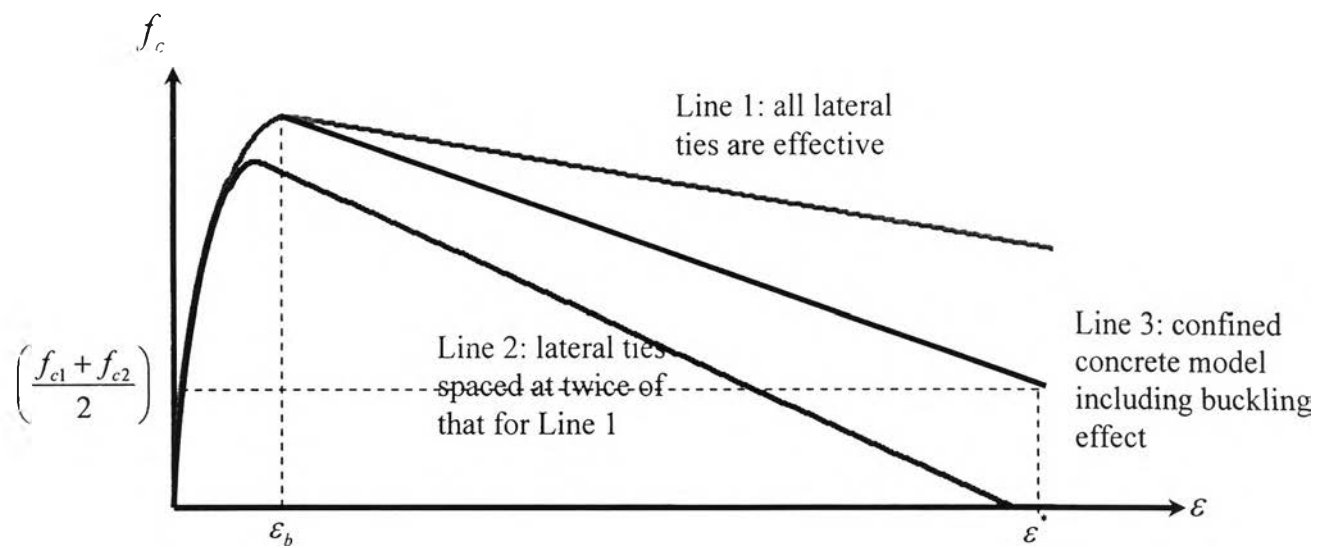


Fig. 3.8 Confined concrete model including buckling effect

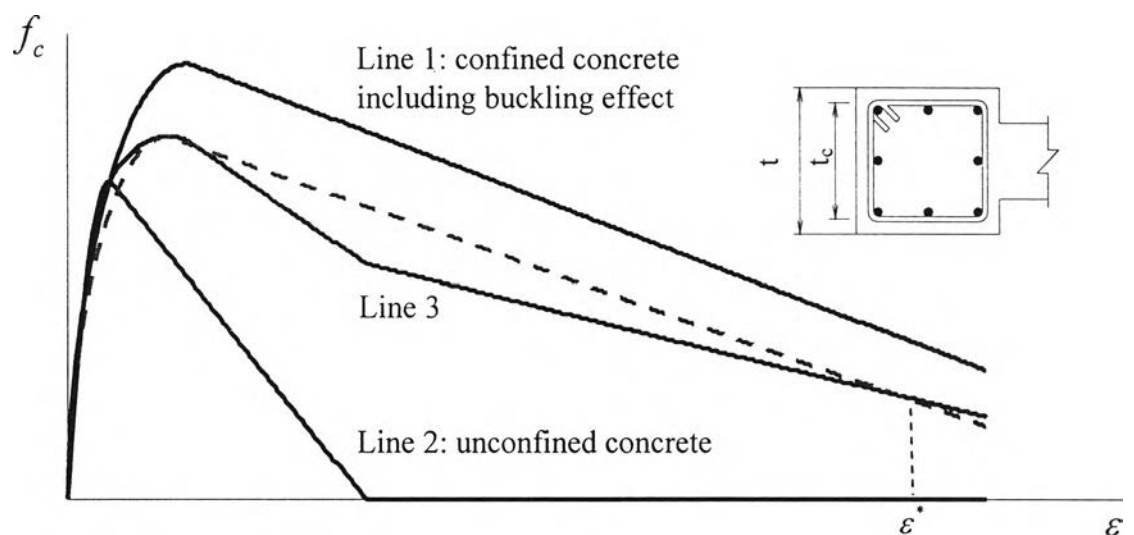


Fig 3.9 Confined concrete model including buckling effect and cover concrete spalling

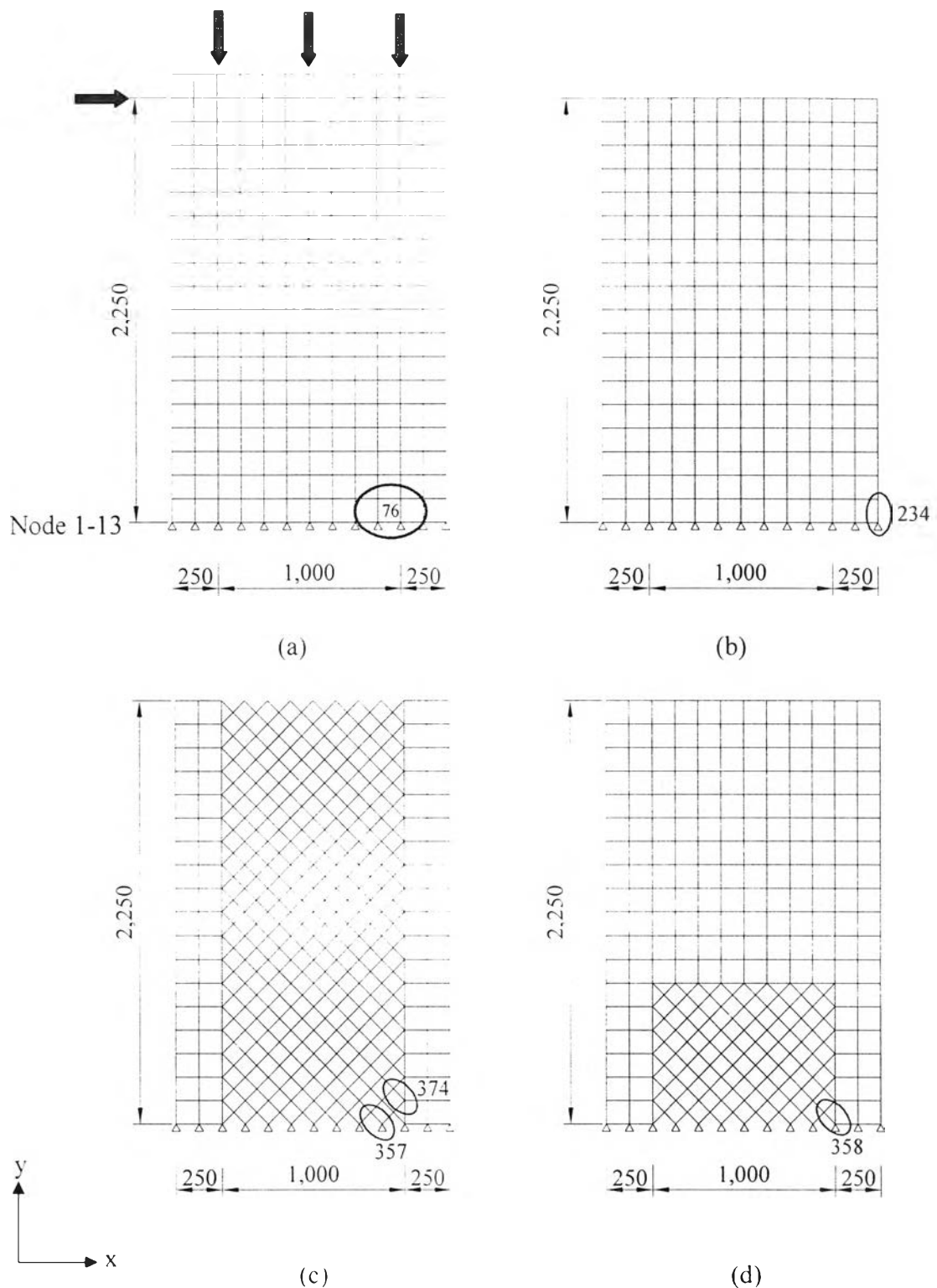


Fig. 3.10 Finite element models: (a) concrete elements; (b) steel elements for wall with conventional web reinforcement; (c) steel elements for wall with diagonal web reinforcement; (d) steel elements for wall with mixed web reinforcement

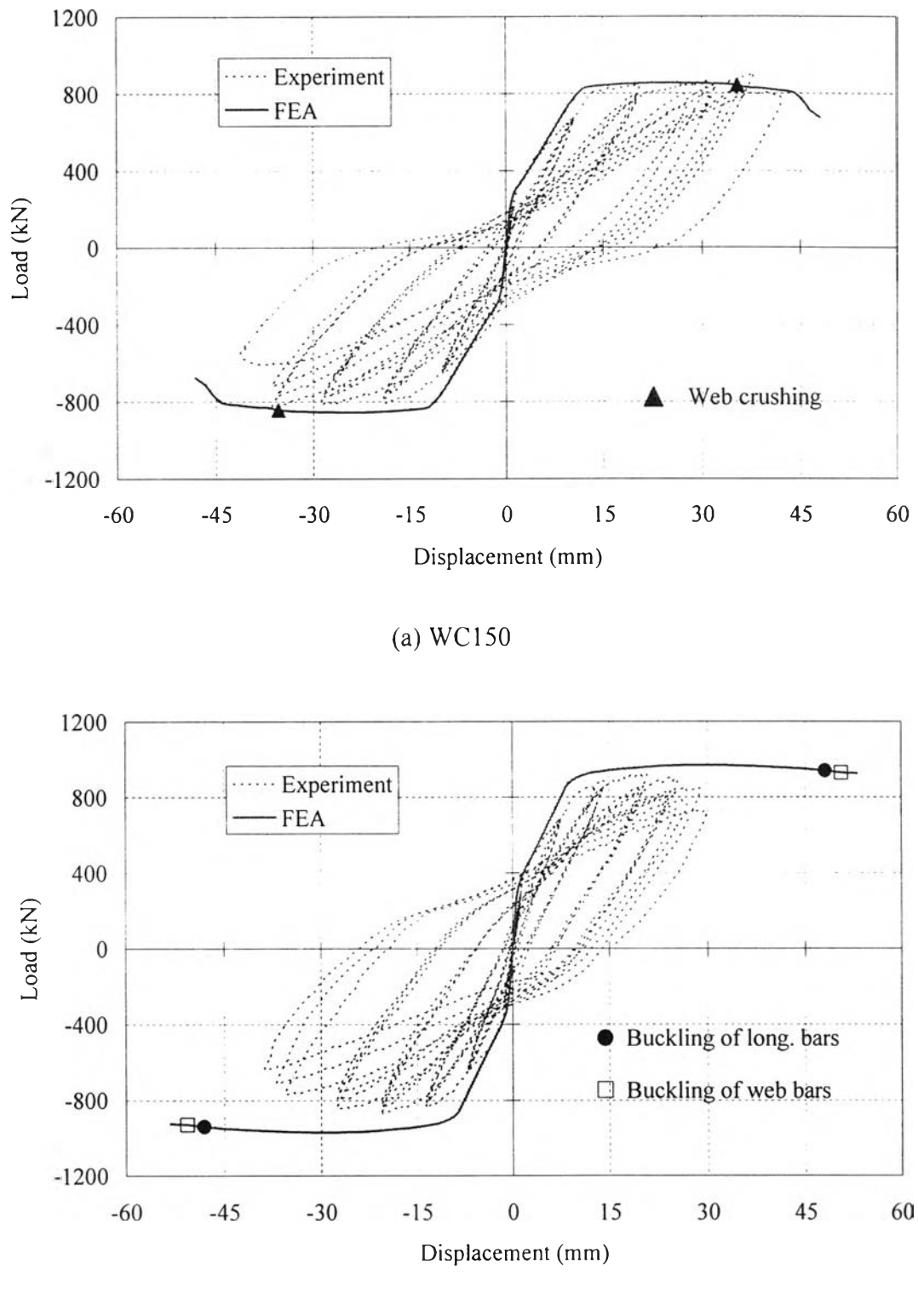
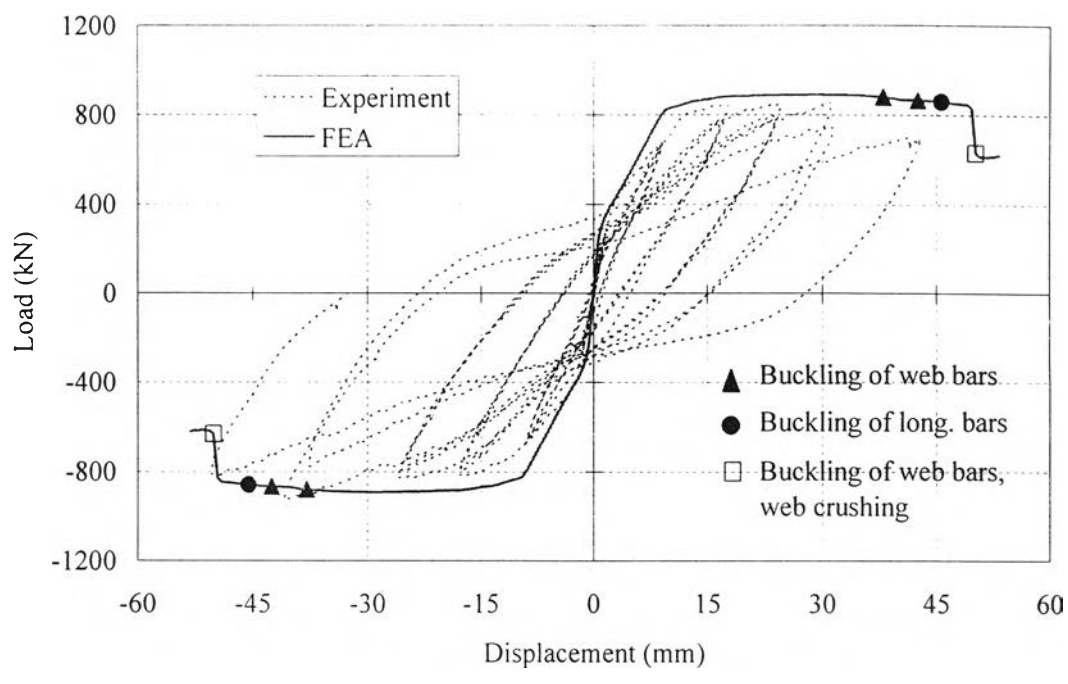
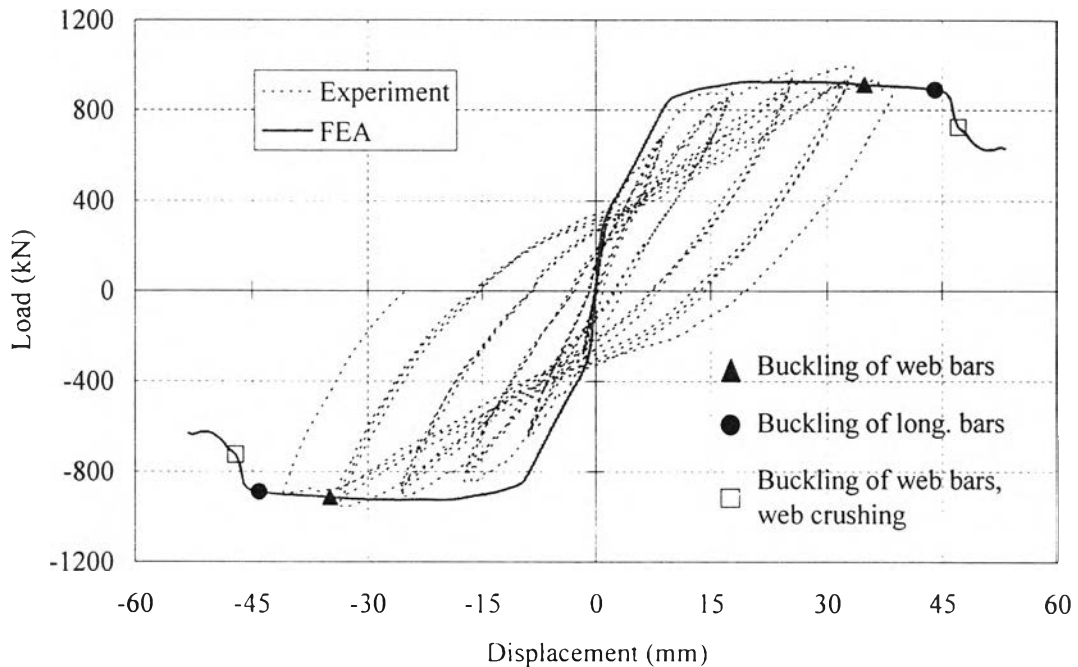


Fig. 3.11 Load-displacement relationships (FEA vs Experiment):

(a) WC150; (b) WD150



(c) WD200



(d) WD170

Fig. 3.11 Load-displacement relationships (FEA vs Experiment) (continue):

(c) WD200; (d) WD170

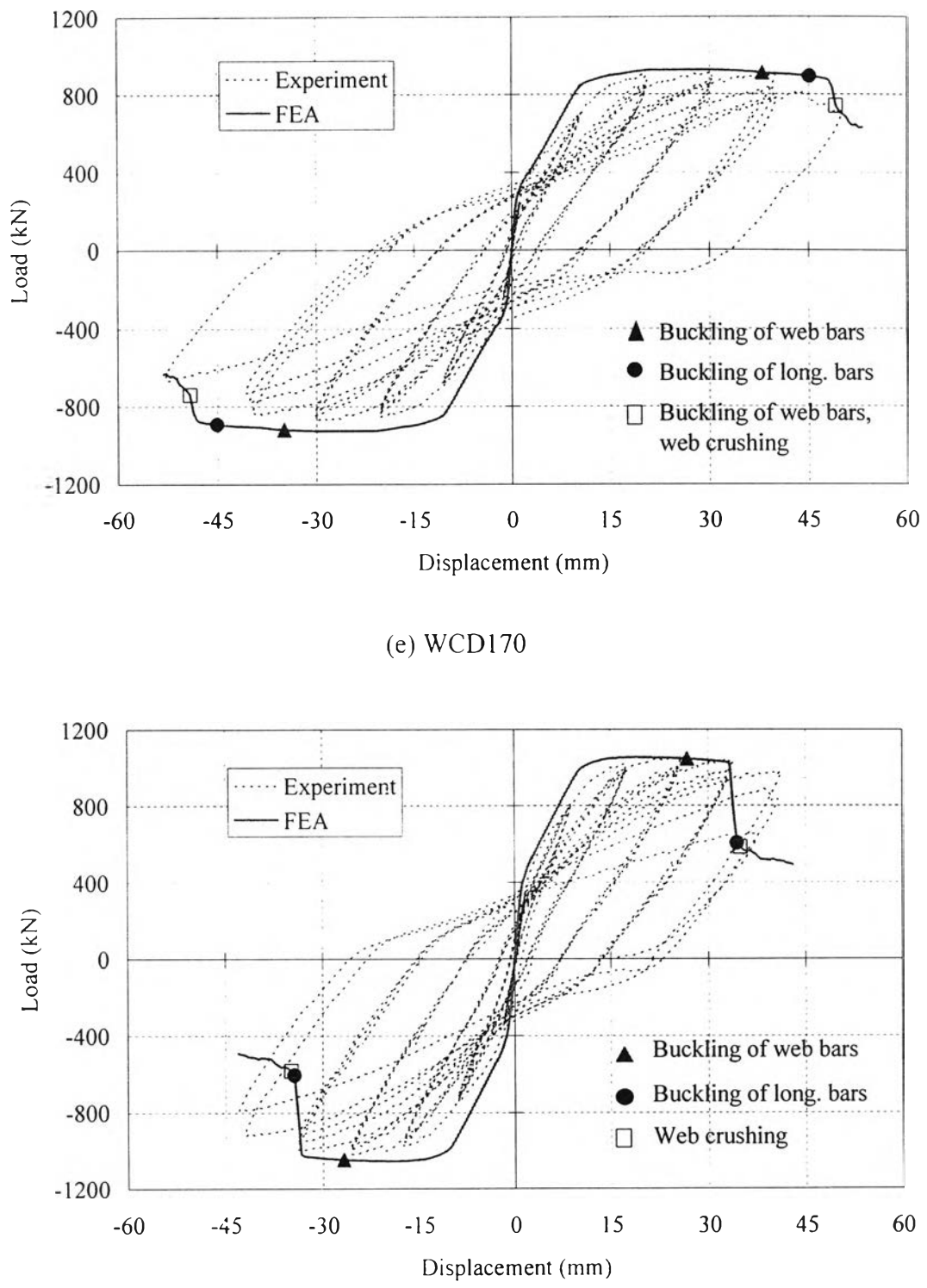
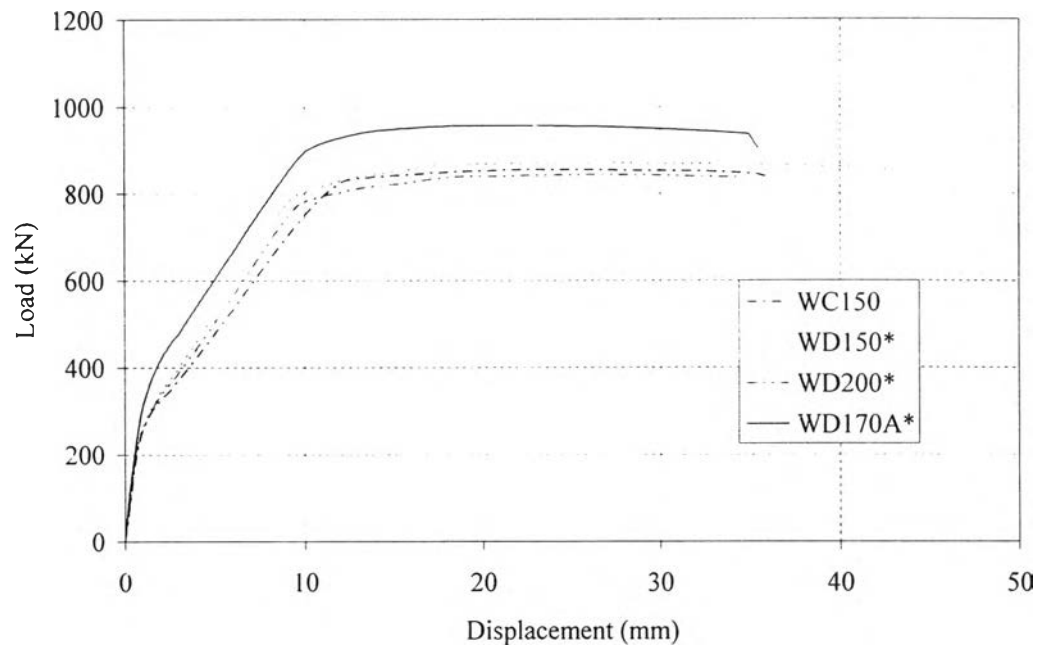
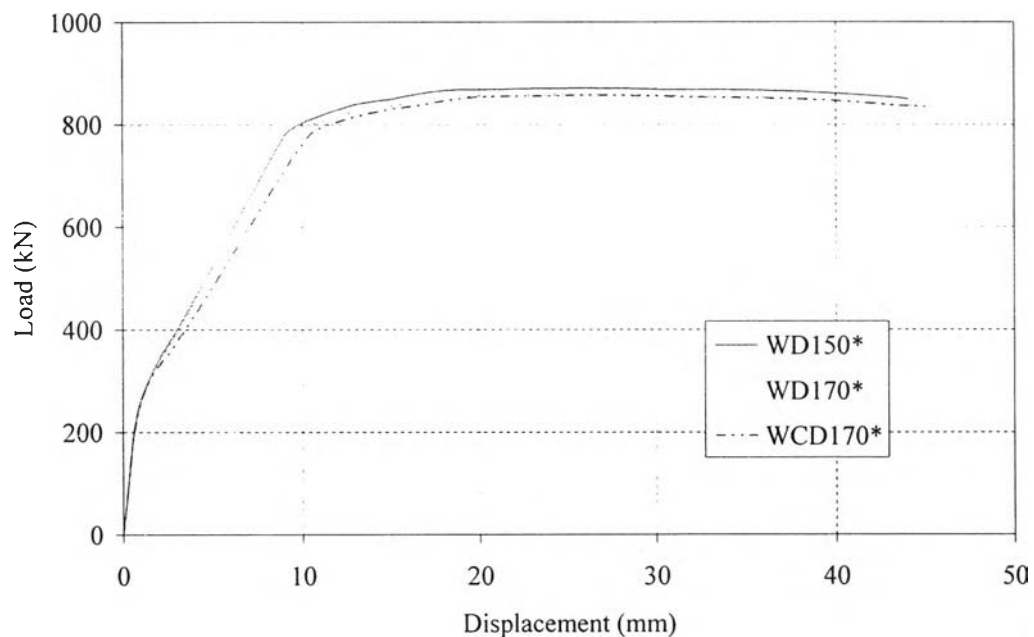


Fig. 3.11 Load-displacement relationships (FEA vs Experiment) (continue):

(e) WCD170; (f) WD170A



(a) Specimens WC150, WD150*, WD200*, and WD170A*



(a) Specimens WD150*, WD170*, and WCD170*

Fig. 3.12 Load-displacement relationships of specimens using the same material properties of specimen WC150

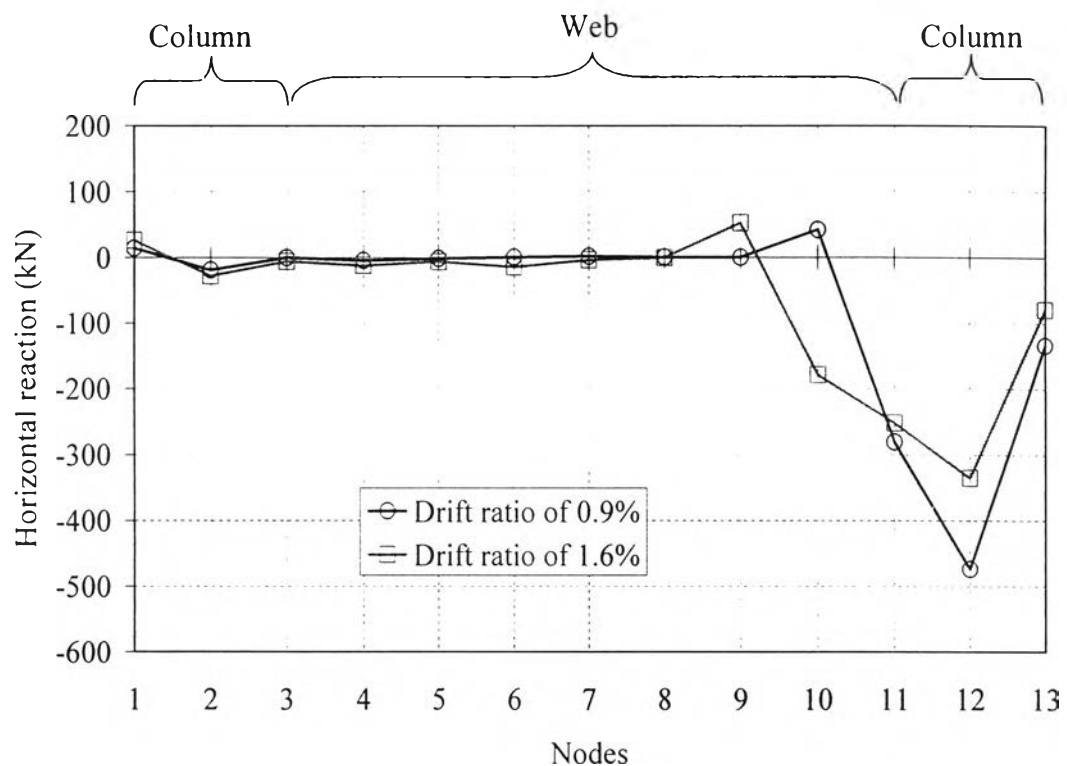


Fig. 3.13 Reaction in horizontal direction of specimen WC150

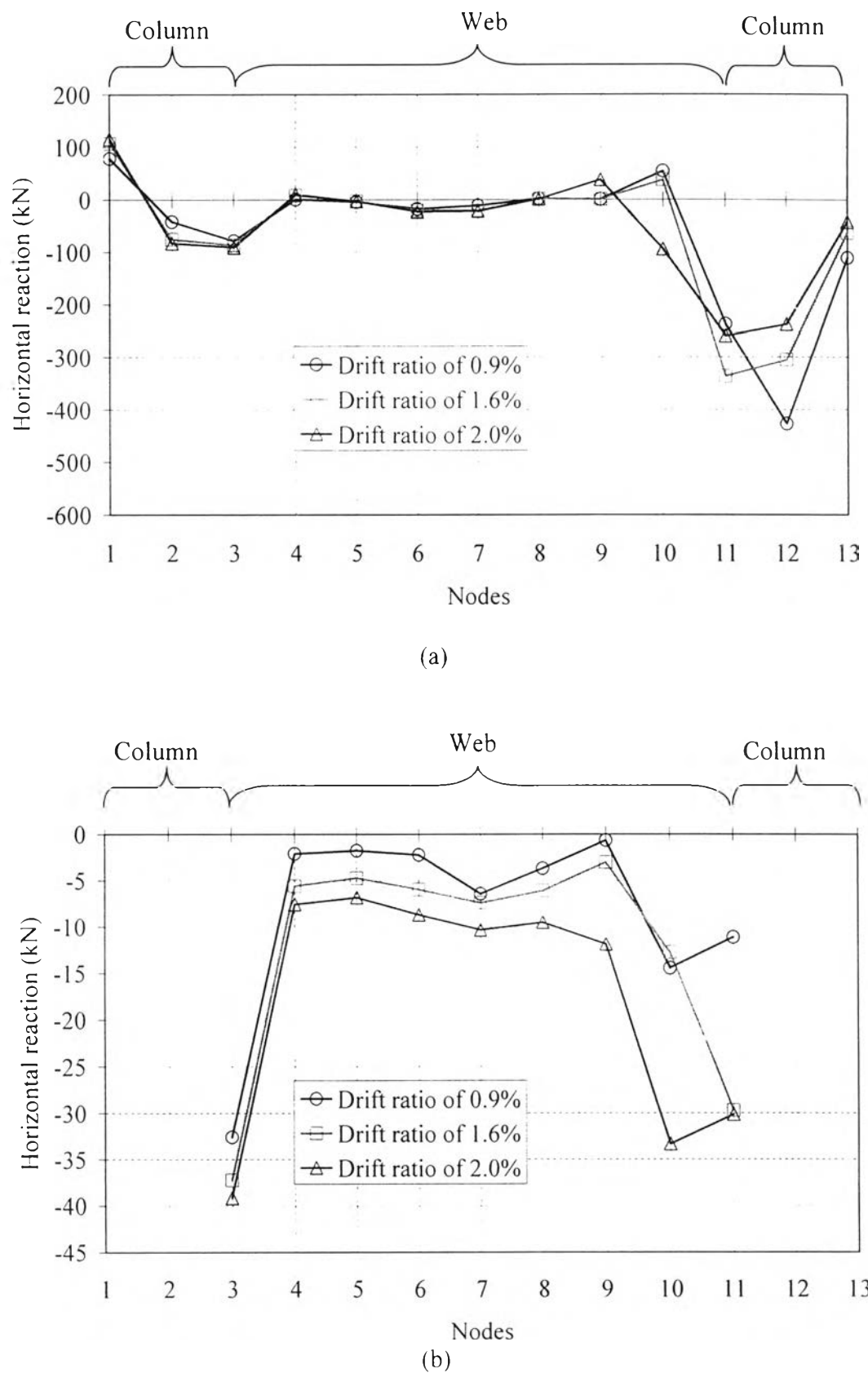


Fig. 3.14 Reaction in horizontal direction of specimen WD150^{*}:

(a) due to concrete (b) due to diagonal web bars

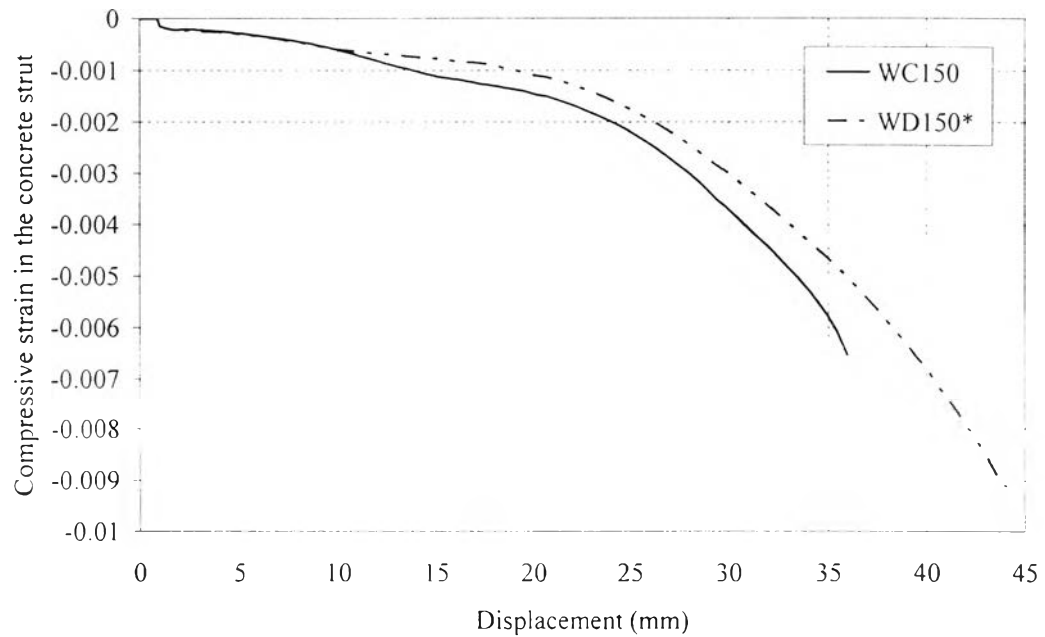


Fig. 3.15 Compressive strain in concrete strut of element 76

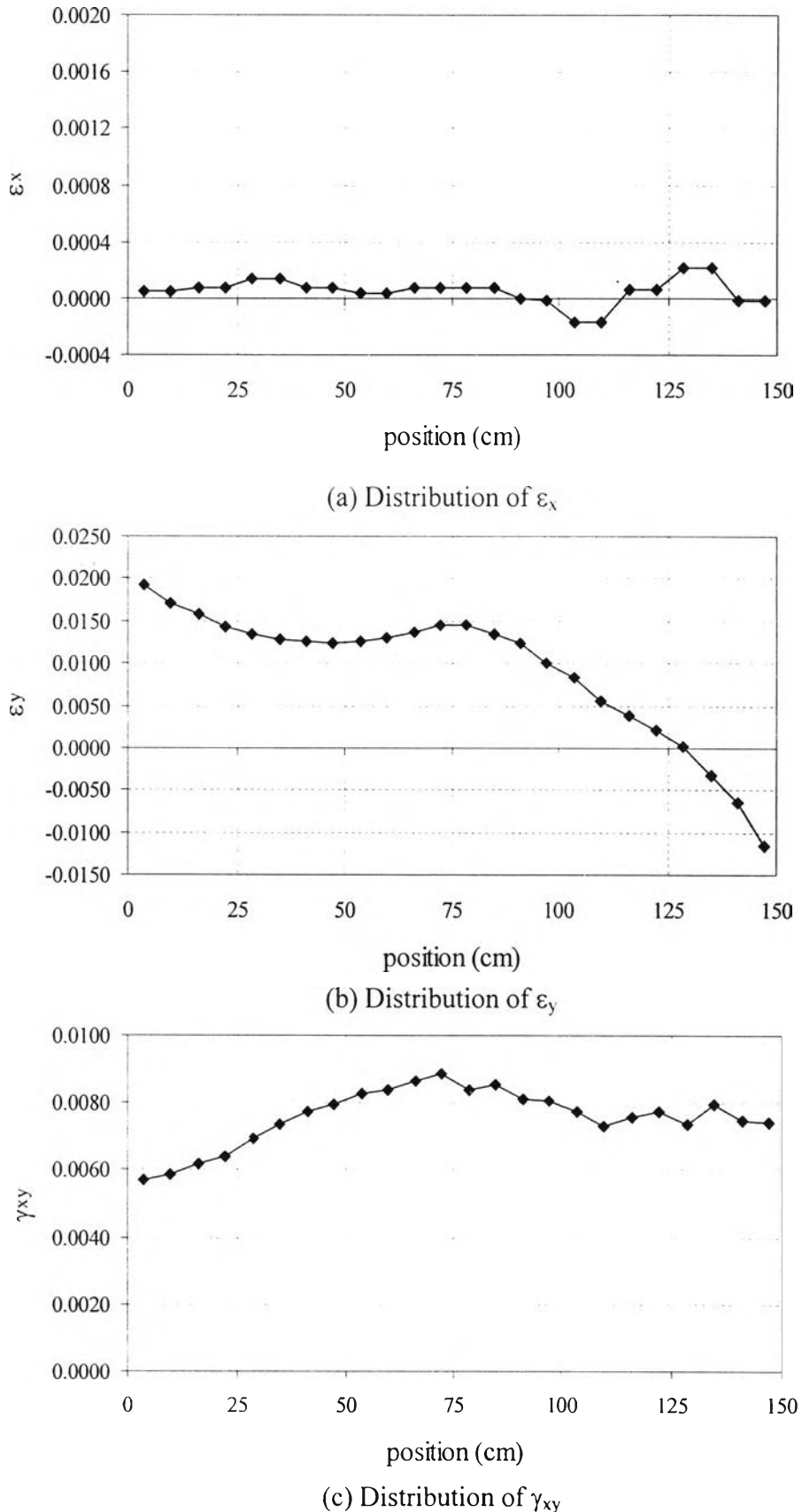


Fig. 3.16 Distributions of strains in concrete of specimen WC150
at the section of the base

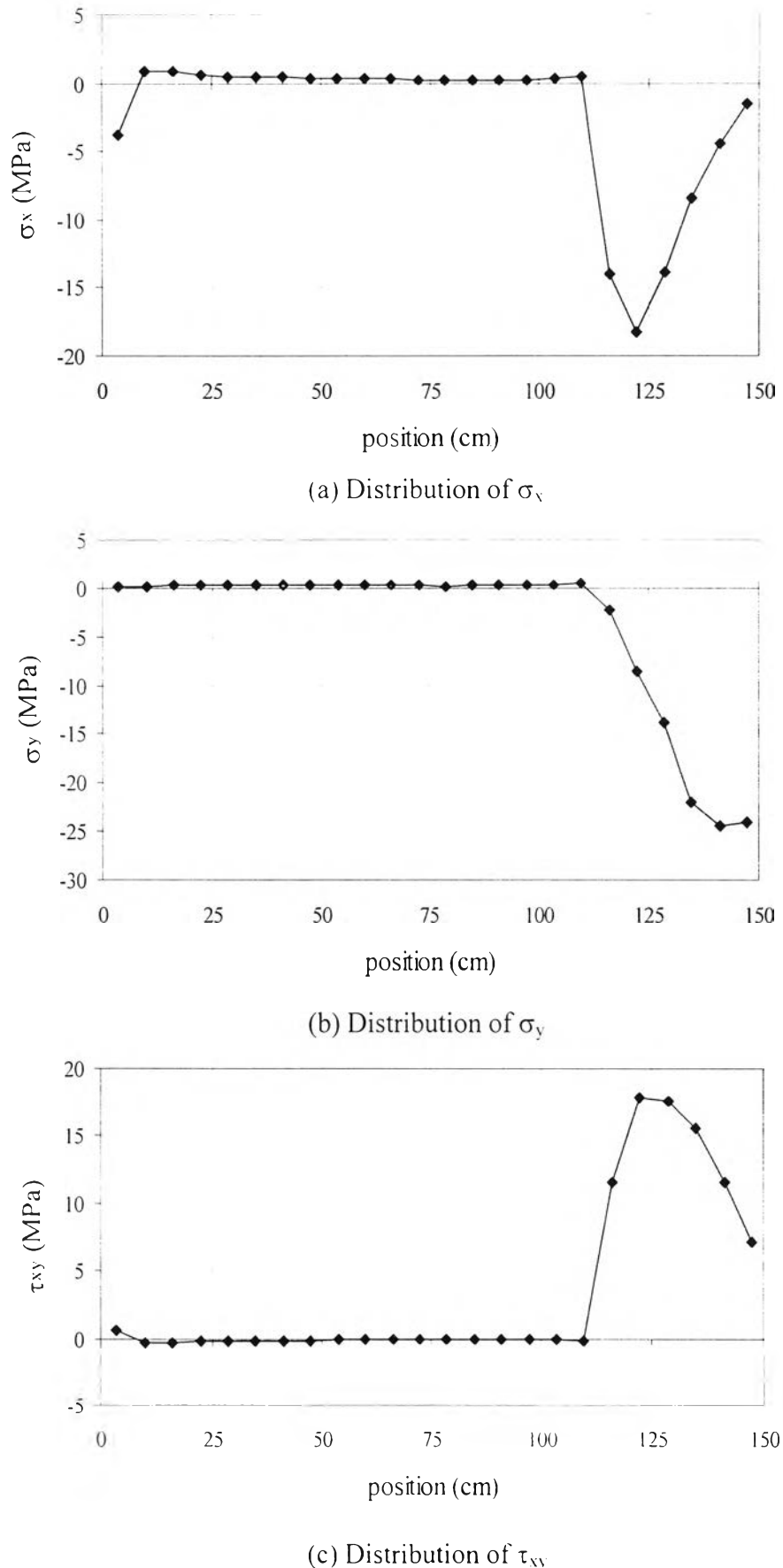


Fig. 3.17 Distributions of stresses in concrete of specimen WC150
at the section of the base

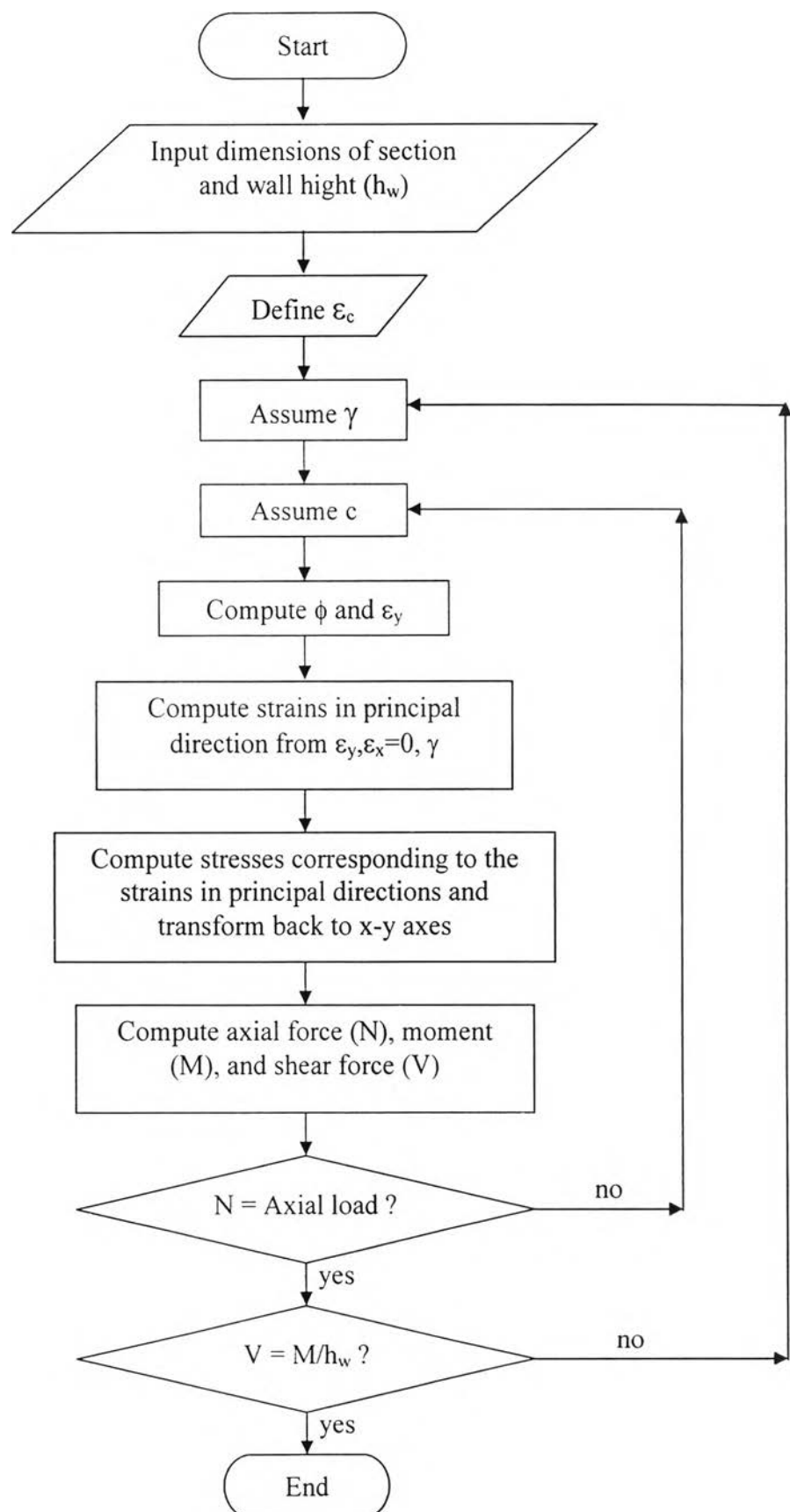


Fig. 4.1 Flowchart for sectional analysis with shear effect

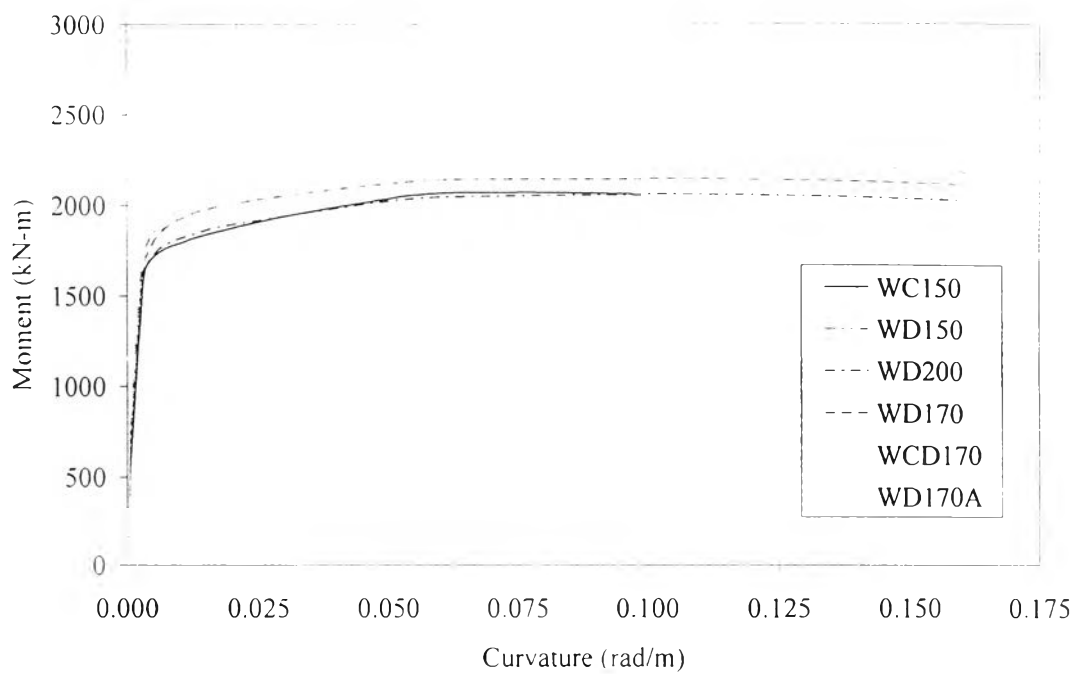


Fig. 4.2 Moment-curvature relationships from sectional analyses

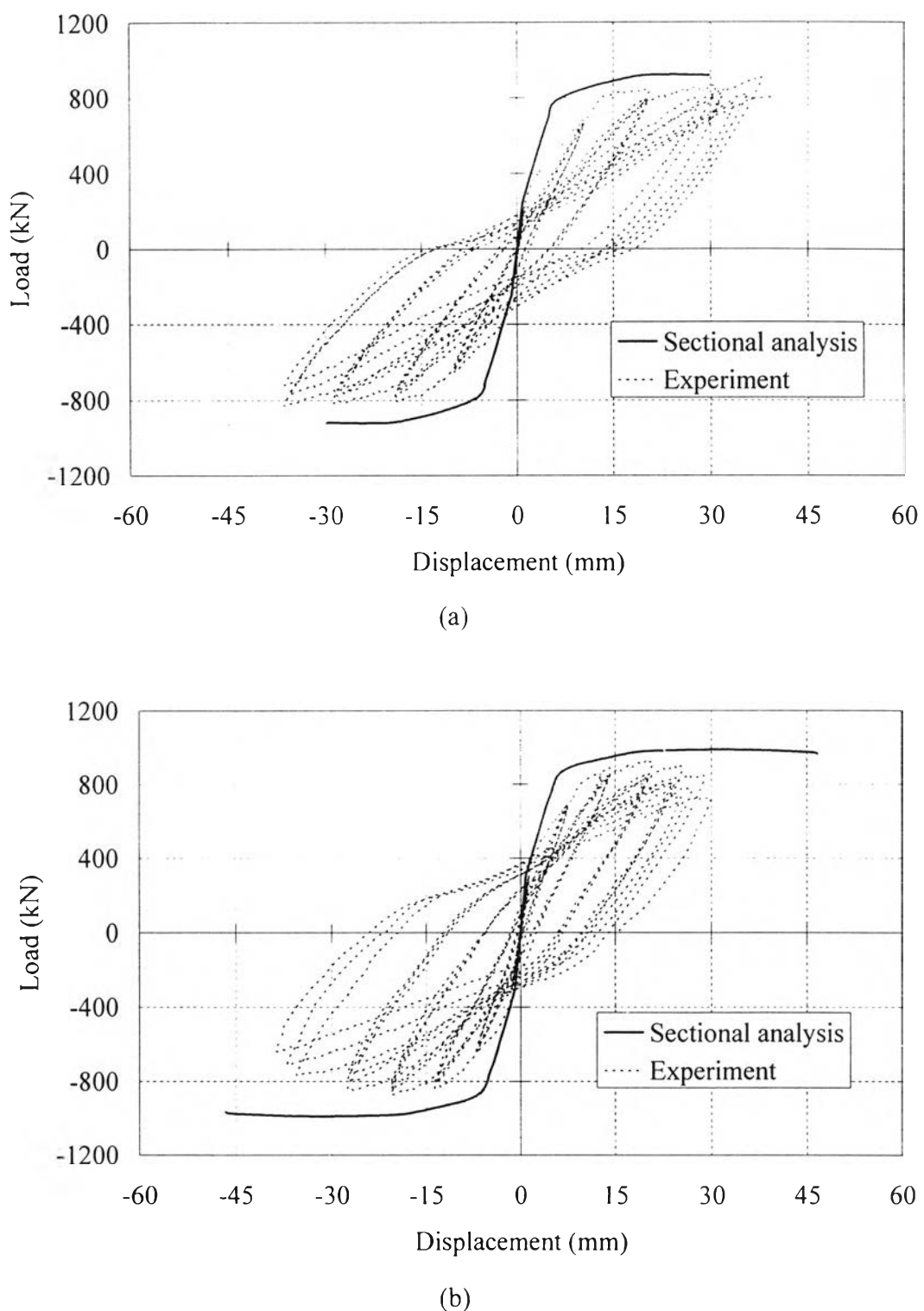


Fig. 4.3 Load-displacement relationships from sectional analyses:

(a) WC150; (b) WD150

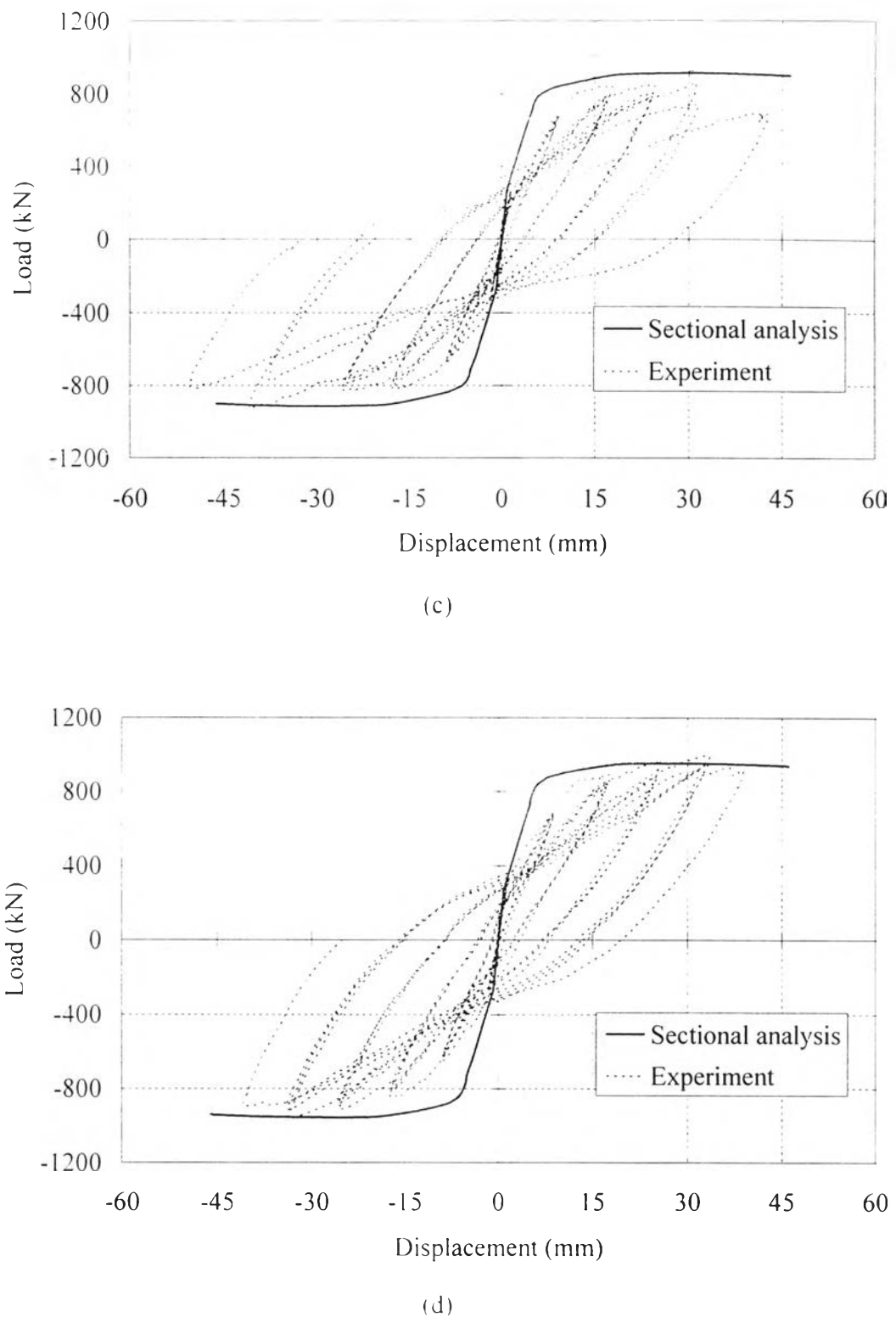


Fig. 4.3 Load-displacement relationships from sectional analyses:
(c) WD200; (d) WD170

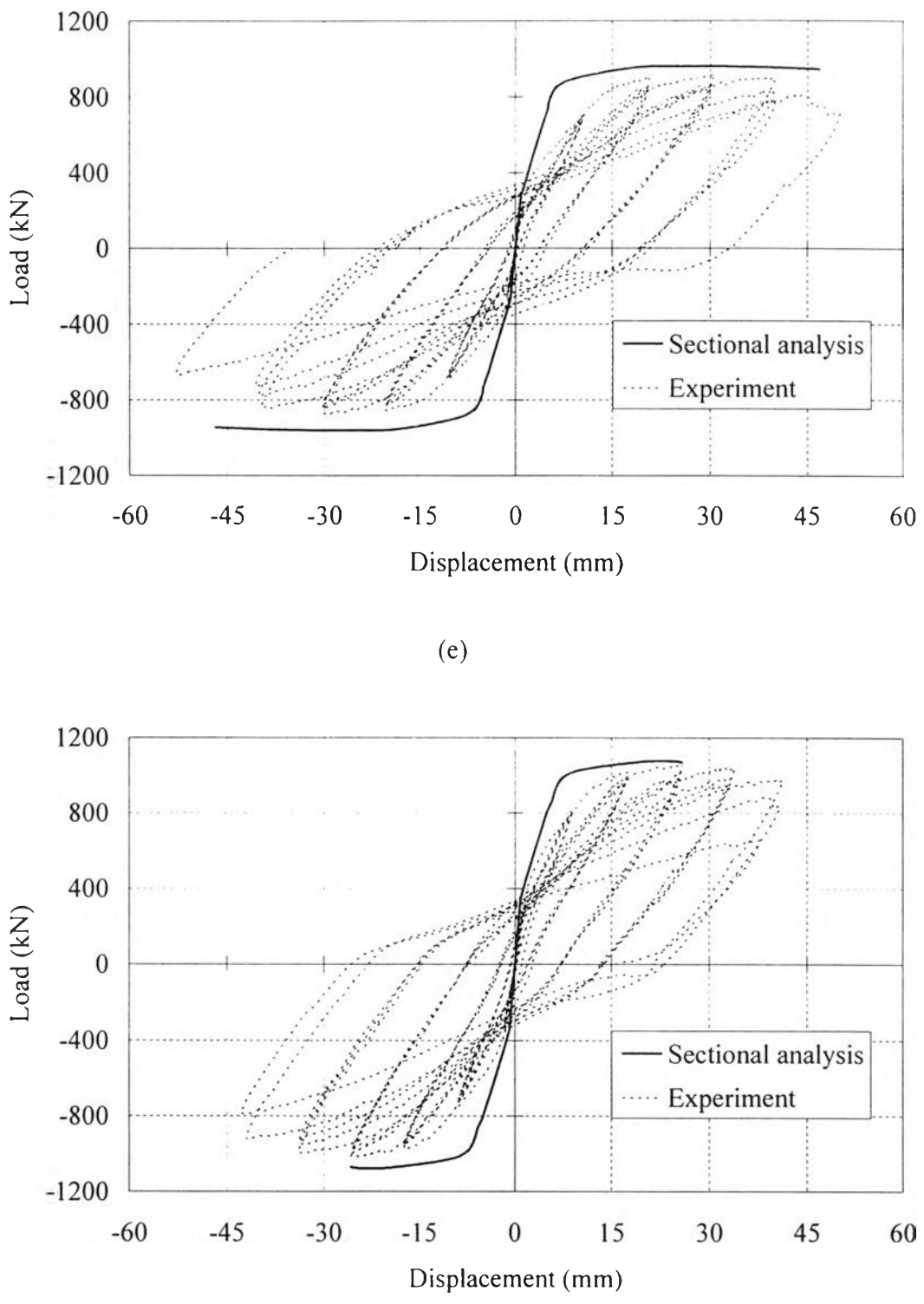


Fig. 4.3 Load-displacement relationships from sectional analyses:
(e) WCD170; (f) WD170A